

X-525-64-343

NASA TMX-55126

AN ANALYSIS  
OF  
SIMULTANEOUS BEAM FORMATION  
BY MEANS OF  
PASSIVE SCATTERING MATRICES  
AND  
UNIFORM PLANAR ANTENNA ARRAYS

FACILITY FORM 602

N65 17259	(ACCESSION NUMBER)	(THRU)
68	(PAGES)	1
TMX-55126	(NASA CR OR TMX OR AD NUMBER)	07
		(CATEGORY)

NOVEMBER 1964

GPO PRICE \$ \_\_\_\_\_

OTS PRICE(S) \$ \_\_\_\_\_

Hard copy (HC) 3.00

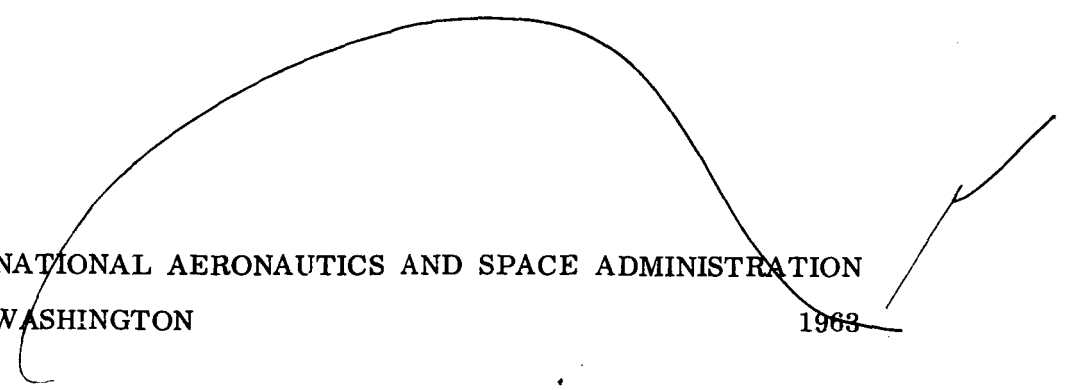
Microfiche (MF) .75



GODDARD SPACE FLIGHT CENTER  
GREENBELT, MARYLAND

AN ANALYSIS OF  
SIMULTANEOUS BEAM FORMATION  
BY MEANS OF PASSIVE SCATTERING MATRICES  
AND UNIFORM PLANAR ANTENNA ARRAYS

R. F. SCHMIDT  
GODDARD SPACE FLIGHT CENTER  
GREENBELT, MARYLAND



NATIONAL AERONAUTICS AND SPACE ADMINISTRATION  
WASHINGTON

1963

AN ANALYSIS OF  
SIMULTANEOUS BEAM FORMATION BY MEANS OF  
PASSIVE SCATTERING MATRICES  
AND UNIFORM PLANAR ANTENNA ARRAYS

By  
R. F. Schmidt

Abstract

17259

The subject report discusses a general three-dimensional crystal-lattice diffraction analysis for uniform planar antenna arrays and treats, in particular, arrays whose lattice phase gradients are determined by an image plane and simultaneous beam-forming matrices composed only of coupler hybrid junctions and fixed phase shifters. A large selection of array problems is discussed in a unified manner by means of lattice notation and the scattering matrix concept. Spatial coordinates of antenna beam maxima and nulls are located directly by means of expressions resembling M. von Laue's crystal diffraction equations. The subject of array gain is related to the surface integral  $\int \mathbf{E}^2(\theta, \varphi) \sin \theta d\theta d\varphi$ . Topics such as grating-lobe formation, cosine-order beams, and beams in the "invisible" region are treated with relative ease. Weighted addition of beams is also considered with a view toward side-lobe level reduction for simultaneous beam-forming matrices, continuous beam steering, and dual-plane phased array monopulse angle tracking.

This report represents an attempt to formulate the uniform planar phased array problem and the multiple-beam matrix concept for purposes of machine calculation. The scattering matrix notation introduced herein provides an organized analysis of beam-forming circuits. It is possible to convert the scattering matrix to a transfer matrix which admits chain multiplication for tandem circuits, thereby providing a method for handling circuits of greater complexity. The report is by no means complete and treats only a few simple scattering circuits. It is, however, a point of departure for a more general investigation of scattering junctions, circuit topology, and inertialess or electronic antenna beam scanning by a purely passive technique.

*R. F. Schmidt*

## CONTENTS

Abstract. . . . .	iii
INTRODUCTION . . . . .	1
DIFFRACTION MODEL . . . . .	3
LATTICE NOTATION . . . . .	8
ARRAY GAIN . . . . .	13
VON LAUE EQUATIONS . . . . .	17
BEAM MAXIMA, MINIMA, AND CROSSOVER LEVELS UNDER ORTHOGONALITY CONDITIONS. . . . .	24
SIMPLE SCATTERING MATRICES . . . . .	32
COMPOSITE SCATTERING MATRICES . . . . .	35
BEAM COMBINING. . . . .	41
APERTURE ILLUMINATION. . . . .	45
CONCLUSION . . . . .	49
ACKNOWLEDGMENTS . . . . .	51
References . . . . .	51

AN ANALYSIS OF  
SIMULTANEOUS BEAM FORMATION BY MEANS OF PASSIVE  
SCATTERING MATRICES AND UNIFORM PLANAR ARRAYS

by

R. F. Schmidt

INTRODUCTION

The subject of simultaneous beam formation from a single aperture has received considerable attention due to (1) the inherent advantages accruing from redundant use of the same antenna structure, (2) the inertialess scanning feature which eliminates physical rotation of large-aperture structures, and (3) the track-while-scan capability for a multiple target situation. Although high data rate systems are frequently associated with ballistic-missile saturation attacks and related tactical problems, it is evident that simultaneous beam formation offers numerous advantages and additional degrees of freedom for satellite tracking and telemetry data reception. Some of the constraints imposed in the tactical radar case can be removed for satellite and spacecraft problems. For example, the target analogue ordinarily carries a beacon or transponder and the array complexity introduced by short-pulse utilization is eliminated. The approach to multiple satellite tracking outlined is considerably simplified. Transient array analysis is considered to be beyond the scope of this report.

The principal objective of this report is to present the general three-dimensional crystal diffraction notation and apply it to studies of uniform planar

antenna arrays placed over perfectly conducting ground planes, a particular set of three-dimensional problems. Actually, numerous uniform array problems can be solved in an organized manner by means of the general diffraction analysis, and several advantages accrue from this rather formal approach. Some of these are the computing and plotting of far-field radiation patterns by machine methods, and the determination of total radiation by means of surface integrals to determine precise directive gain values for an array. The general three-dimensional analysis presented in this report draws heavily upon sources in the classical literature. Various assumptions and idealizations under which the analysis presented is valid are discussed in detail.

The analysis is shown to provide a high order of flexibility for studying arbitrarily large arrays, and admits variation of such parameters as the array phase gradients, the element separation, the free-space element pattern, and the height of the source element above the reflector. Calculation of the angular coordinates of the principal beam maxima is achieved without mapping the complete radiation patterns, although the detailed three-dimensional Fraunhofer patterns can be obtained directly from simple source and lattice factors. The beam principal maxima and minima are located by means of von Laue type diffraction equations which, when satisfied, lead to simultaneous maximization of certain lattice factors. Using the same general three-dimensional crystal notation, the origin and significance of grating lobes is discussed in relation to so-called spurious (non-visible) beam conditions which can arise for planar arrays. The subject of array phase centers is introduced and an expression is derived for the requisite phase corrections when two or more beams are combined

by redundant utilization of a linear or planar aperture to form simple sum, difference, and cosine-order beams.

A certain amount of material pertaining to hybrid junctions and scattering matrices is introduced subsequent to presenting the crystal lattice notation to make the application of the lattice notation specific. The array phase gradients are determined by particular forms of scattering matrices which, to a certain extent, predetermines the solutions for the far-field radiation patterns. The scattering matrix concept is shown to provide a convenient means of displaying linear and planar array gradients which greatly facilitates multiport circuit analysis. Basic hybrid building-blocks of the corporate feeds and the complex feeds themselves are described in terms of mathematical matrices whose individual elements represent reflection coefficients and transmission coefficients of definite amplitude and phase. A linear ( $16 \times 1$ ) scattering matrix is presented in detail. The corresponding simple sum beam (first-order cosine beam), the difference beam, and the aperture illumination (current distribution) are then formed to illustrate the application of the notation.

## DIFFRACTION MODEL

Since there exists a remarkably close analogy between x-ray diffraction analysis and antenna array theory, the methods developed for crystal structure analysis are in large part applicable to antenna design. The x-ray diffraction problem, simply stated, is one of determining the location of the atomic dipoles in a crystal-lattice structure from diffraction spectra consisting of intensity information only. The antenna array problem is one of determining a radiation pattern corresponding to particular lattice spacings and prescribed phase

conditions among the source elements. References pertaining to the crystal-lattice approach, as adapted to antenna analysis, can be found in the textbooks of Stratton<sup>1</sup> and Silver.<sup>2</sup> In order to facilitate the discussion the notation of Stratton will be used throughout this report wherever the lattice analysis appears.

Certain assumptions are fundamental to the determination of far-field radiation patterns by means of diffraction analysis. Among these is the assumption that the constitutive parameters are independent of field strength, which ensures the linearity of the constitutive equations and Maxwell's equations. That is, if the conductivity  $\sigma$ , electric inductive capacity  $\epsilon$ , and magnetic inductive capacity  $\mu$  are independent of field strength, then the superposition of fields is admissible. A set of electric and magnetic field vectors  $\bar{E}_1$  and  $\bar{H}_1$ , due to charge and current source functions  $\rho_1$  and  $\bar{J}_1$ , satisfies the field equations. This set can be summed with a similar set  $\bar{E}_2$  and  $\bar{H}_2$ , due to  $\rho_2$  and  $\bar{J}_2$ , which also satisfies the field equations. Then  $\bar{E} = \bar{E}_1 + \bar{E}_2$ ,  $\bar{H} = \bar{H}_1 + \bar{H}_2$ ,  $\rho = \rho_1 + \rho_2$  and  $\bar{J} = \bar{J}_1 + \bar{J}_2$  is a superposition which is consistent with Maxwell's equations and which describes a possible electromagnetic field. The subject of antenna gain is closely associated with this notion, as will appear later.

Another assumption ordinarily taken into the diffraction analysis is that the radial distance  $r$  from a source element  $S_j$  to the far-field point  $P$  is given by

$$r = R - \bar{r}_j \cdot \bar{R}_0. \quad (1)$$

The vectors from coordinate origin to radiator, radiator to field point, and origin to field point are given by  $\bar{r}_j$ ,  $\bar{r}$  and  $\bar{R}$  respectively as shown in Figure 1, and  $\bar{R}_0 = \bar{R}/|\bar{R}|$ , a unit vector. This notation will be consistent throughout the discussion.



The inference of Eq. (1) is that  $\bar{r} \times \bar{R} = 0$ , or  $\bar{r}$  and  $\bar{R}$  are parallel for the field point. Superposition of the component fields contributed by sources (1) with separate current distributions and (2) occupying a finite region of space leads to quasi-point-source fields. The far fields obtained in this manner are not point-source fields since the equiphase

surfaces are not the family of spheres of constant radius  $R$ , in general, even if the individual sources are true point-source radiators. A rather lengthy argument is required to develop the expressions for the far-field resulting from a multiplicity of sources if Maxwell's equations are taken as the starting point. The text by Silver<sup>3</sup> treats this problem rigorously and in considerable detail. It is sufficient here to state that the far-zone fields at a point  $P$  have the form

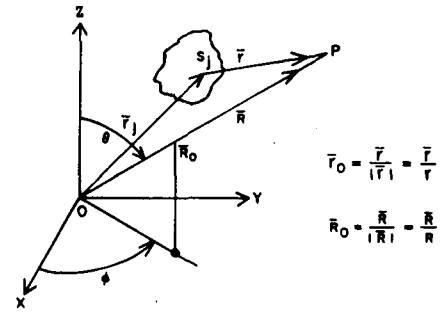


Figure 1-Origin of coordinates, source, and field points.

$$\begin{aligned} \bar{E}_p = -\frac{i\omega\mu}{4\pi R} e^{-ikR} \int_v \left[ \bar{J} - (\bar{J} \cdot \bar{R}_0) \bar{R}_0 + \left(\frac{\epsilon}{\mu}\right)^{1/2} \bar{J}_m \times \bar{R}_0 \right] e^{+ik\bar{r}_j \cdot \bar{R}_0} dv \\ + 0 \left(\frac{1}{R^2}\right) + 0 \left(\frac{1}{R^3}\right) \end{aligned} \quad (2)$$

and

$$\begin{aligned} \bar{H}_p = -\frac{i\omega\epsilon}{4\pi R} e^{-ikR} \int_v \left[ \bar{J}_m - (\bar{J}_m \cdot \bar{R}_0) \bar{R}_0 - \left(\frac{\mu}{\epsilon}\right)^{1/2} \bar{J} \times \bar{R}_0 \right] e^{+ik\bar{r}_j \cdot \bar{R}_0} dv \\ + 0 \left(\frac{1}{R^2}\right) + 0 \left(\frac{1}{R^3}\right) \end{aligned} \quad (3)$$

under

$$\mathbf{r} = \mathbf{R} - \bar{\mathbf{r}}_j \cdot \bar{\mathbf{R}}_0,$$

where the new terms are:

$\bar{\mathbf{J}}_m$  = the magnetic current density; a formalism taken to be zero, generally,  
but retained here for symmetry purposes.

$$\omega = 2\pi f$$

$f$  = frequency

$$k = \frac{2\pi}{\lambda}$$

$\lambda$  = wavelength

$$i = \sqrt{-1}$$

The volume integrals are independent of  $\mathbf{r}$ , ensuring that  $R\bar{\mathbf{E}}_p$  and  $R\bar{\mathbf{H}}_p$  remain finite as the radius of the sphere of observation approaches infinity ( $R \rightarrow \infty$ ).

Since  $\bar{\mathbf{E}}$  and  $\bar{\mathbf{H}}$  satisfy the radiation conditions

$$\lim_{R \rightarrow \infty} R \left[ \left( \bar{\mathbf{R}}_0 \times \bar{\mathbf{H}} \right) + \left( \frac{\epsilon}{\mu} \right)^{1/2} \bar{\mathbf{E}} \right] = 0 \quad (4)$$

and

$$\lim_{R \rightarrow \infty} R \left[ \left( \frac{\epsilon}{\mu} \right)^{1/2} (\bar{\mathbf{R}}_0 \times \bar{\mathbf{E}}) - \bar{\mathbf{H}} \right] = 0 \quad (5)$$

the radiative components of  $\bar{\mathbf{E}}$  and  $\bar{\mathbf{H}}$  are mutually perpendicular and both normal to  $\bar{\mathbf{R}}_0$ .

At this point of the development, it is sufficient to consider only the  $\bar{\mathbf{E}}$  fields since radiation has now been established, and it is helpful to resolve the  $\bar{\mathbf{E}}$  field of Eq. (2) into  $\theta$  and  $\phi$  components in a spherical coordinate system. Then, if  $\hat{\mathbf{i}}_\theta, \hat{\mathbf{i}}_\phi$  are unit vectors,

$$\bar{\mathbf{E}}_p = E_\theta \hat{\mathbf{i}}_\theta + E_\phi \hat{\mathbf{i}}_\phi \quad (6)$$

where

$$\begin{aligned} E_\theta = \bar{\mathbf{E}}_p \cdot \hat{\mathbf{i}}_\theta &= -\frac{i\omega\mu}{4\pi R} e^{-ikR} \int_V \left[ \bar{\mathbf{J}} \cdot \hat{\mathbf{i}}_\theta + \left(\frac{\epsilon}{\mu}\right)^{1/2} \bar{\mathbf{J}}_m \cdot \hat{\mathbf{i}}_\phi \right] e^{ik\bar{\mathbf{r}}_j \cdot \bar{\mathbf{R}}_0} dv \\ &= -\frac{i\omega\mu}{4\pi R} e^{-ikR} F_1(\theta, \phi) \end{aligned} \quad (7)$$

and

$$\begin{aligned} E_\phi = \bar{\mathbf{E}}_p \cdot \hat{\mathbf{i}}_\phi &= -\frac{i\omega\mu}{4\pi R} e^{-ikR} \int_V \left[ \bar{\mathbf{J}} \cdot \hat{\mathbf{i}}_\phi - \left(\frac{\epsilon}{\mu}\right)^{1/2} \bar{\mathbf{J}}_m \cdot \hat{\mathbf{i}}_\theta \right] e^{ik\bar{\mathbf{r}}_j \cdot \bar{\mathbf{R}}_0} dv \\ &= -\frac{i\omega\mu}{4\pi R} e^{-ikR} F_2(\theta, \phi) \end{aligned} \quad (8)$$

since

$$\bar{\mathbf{J}}_m \times \bar{\mathbf{R}}_0 \cdot \hat{\mathbf{i}}_\theta = \bar{\mathbf{J}}_m \cdot \hat{\mathbf{i}}_\phi \quad (9)$$

and

$$\bar{\mathbf{J}}_m \times \bar{\mathbf{R}}_0 \cdot \hat{\mathbf{i}}_\phi = -\bar{\mathbf{J}}_m \cdot \hat{\mathbf{i}}_\theta \quad (10)$$

The diffraction analysis for a planar array can now be accomplished by considering the cross-polarized components  $E_\theta, E_\phi$  independently, therefore, the crystal-diffraction analysis will be written for linear polarization only. Composite fields can then be constructed as required by summing the resultant  $E_\theta$  and  $E_\phi$  fields radiated from the array with due regard for their phase relationship.

The amount of complexity introduced into an antenna array analysis depends upon the assumptions admitted for the ensemble of radiators or scatterers. In the case of x-ray crystallography, the scattering cross-section is a small fraction of the area irradiated by the incident wave and the usual assumption is that the scattering from any one center is independent of the presence of other scatterers.<sup>4</sup> Multiple scattering between elements is neglected. This assumption is carried into the present analysis and each element of the array will be considered identical and invariant with scan angle. Each element is also taken to be an interior element of the array, to the exclusion of all edge effects. An equivalent statement is that the array is assumed to be of such an extent that the ratio of peripheral to interior elements is negligibly small. Any interaction which leads to a new set of identical element currents  $I'_{oj}$  will not invalidate the analysis since the original set of currents  $I_{oj}$  is simply replaced by  $I'_{oj}$  which permits a reapplication of the notation. Problems pertaining to power conservation, energy storage in the array, absolute gain, or absolute field intensity require additional attention.

#### LATTICE NOTATION

A planar array of sources exhibiting complex phase patterns, situated over a perfectly conducting ground-plane is a particularly interesting array which can be considered as a three-dimensional lattice of source elements and is one which brings out most of the salient features of the analysis. It will be assumed that the array is uniform in the sense that (1) all of the real and image elements are parallel to one another and carry currents of identical magnitude, (2) the spacing of the elements is uniform but not necessarily equal on each of three orthogonal

coordinate axes, and (3) the phase gradient on each axis is linear, but not necessarily equal for the three principal directions  $\bar{a}_1, \bar{a}_2, \bar{a}_3$  as shown in Figure 2. The result of Eq. (7) can be restated, with some slight modification, to admit complex array elements and to provide for relative phase delays between the array phase gradients. It is convenient to undertake this by noting that the  $j^{\text{th}}$  oscillator in the lattice is located by a vector

$$\bar{r}_j = j_1 \bar{a}_1 + j_2 \bar{a}_2 + j_3 \bar{a}_3$$

as shown in Figure 2; where  $j_1, j_2, j_3$  are integers including zero. It follows that the phase of the  $j^{\text{th}}$  oscillator with respect to the phase of the oscillator at the origin is  $\beta_j$ ,

$$\beta_j = (j_1 \alpha_1 + j_2 \alpha_2 + j_3 \alpha_3) + (\delta_1 + \delta_2 + \delta_3), \quad (11)$$

allowing for phase shifts  $\delta_1, \delta_2, \delta_3$  in the network corresponding to the formation of the gradients  $\alpha_1, \alpha_2, \alpha_3$  respectively. Following Stratton's<sup>5</sup> lattice notation, the radiation field of the  $j^{\text{th}}$  oscillator is

$$E_j = -i 60 I_{oj} F_0(\theta) \frac{e^{ikR - i\omega t - ik\bar{R}_0 \cdot \bar{r}_j - i\beta_j}}{R}, \quad (12)$$

assuming a half-wave oscillator oriented as in Figure 2, where  $\bar{R}_0$  is a unit vector,  $\bar{R}_0 = \bar{R} / |\bar{R}|$ , in the direction  $\bar{R}$  and is consistent with Figure 1. The composite or resultant field for the entire array then becomes

$$E = -i 60 F_0(\theta) \frac{e^{ikR - i\omega t}}{R} \sum_j I_{oj} e^{-i(k\bar{R}_0 \cdot \bar{r}_j + \beta_j)} \quad (13)$$

If the simple half-wave oscillator is replaced by a complex source element, and if one of the  $E_\theta, E_\phi$  fields is considered at a time, then Eq. (13) can be written as

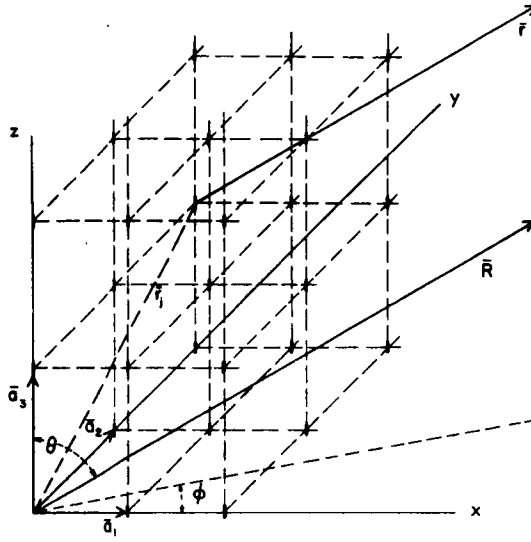


Figure 2—Uniform lattice structure in three dimensions defined by orthogonal base vectors  $\bar{a}_1, \bar{a}_2, \bar{a}_3$ .

$$\mathbf{E} = -i 60 F'_0(\theta) e^{-i g(\theta, \phi)} \frac{e^{i k \mathbf{R}} - i \omega t}{R} \sum_j I_{oj} e^{-i(k \bar{\mathbf{R}}_0 \cdot \bar{\mathbf{r}}_j + \beta_j)} \quad (14)$$

where  $F'_0(\theta)$  represents the amplitude envelope of the free-space field-intensity pattern and  $g(\theta, \phi) = \xi$  is a function which defines the phase-pattern of the complex source element.

Let the number of radiators in any line parallel to the x, y, z axes be  $n_1, n_2, n_3$  respectively, so that the lattice is completely filled, and let the spacings along the coordinate directions be  $a_1 = |\bar{a}_1|$ ,  $a_2 = |\bar{a}_2|$ ,  $a_3 = |\bar{a}_3|$ . Unit vectors are then given by

$$\hat{\mathbf{l}}_x = \frac{\bar{\mathbf{a}}_1}{a_1}, \quad \hat{\mathbf{l}}_y = \frac{\bar{\mathbf{a}}_2}{a_2}, \quad \hat{\mathbf{l}}_z = \frac{\bar{\mathbf{a}}_3}{a_3}$$

and

$$\begin{aligned} \bar{\mathbf{R}}_0 \cdot \bar{\mathbf{r}}_j &= \left[ \sin \theta \cos \phi \left( \frac{\bar{a}_1}{a_1} \right) + \sin \theta \sin \phi \left( \frac{\bar{a}_2}{a_2} \right) + \cos \theta \left( \frac{\bar{a}_3}{a_3} \right) \right] \cdot \left[ j_1 a_1 \left( \frac{\bar{a}_1}{a_1} \right) + j_2 a_2 \left( \frac{\bar{a}_2}{a_2} \right) + \right. \\ &\quad \left. + j_3 a_3 \left( \frac{\bar{a}_3}{a_3} \right) \right] = j_1 a_1 \sin \theta \cos \phi + j_2 a_2 \sin \theta \sin \phi + j_3 a_3 \cos \theta. \end{aligned} \quad (15)$$

Complex lattice factors can now be defined as follows to account for the total field generated by the array of oscillators.

$$f_1 = \sum_{j_1=0}^{n_1-1} e^{-i j_1 (k a_1 \sin \theta \cos \phi + \alpha_1)} \quad (16)$$

$$f_2 = \sum_{j_2=0}^{n_2-1} e^{-i j_2 (k a_2 \sin \theta \sin \phi + \alpha_2)} \quad (17)$$

$$f_3 = \sum_{j_3=0}^{n_3-1} e^{-i j_3 (k a_3 \cos \theta + \alpha_3)} \quad (18)$$

Each lattice factor above has exponentials whose arguments depend upon a spatial term (a projection) and temporal term (a phase gradient). All diffraction phenomena discussed in this report are based on these fundamental expressions.

Let

$$\gamma_1 = k a_1 \sin \theta \cos \phi + \alpha_1 \quad (19)$$

$$\gamma_2 = k a_2 \sin \theta \sin \phi + \alpha_2 \quad (20)$$

$$\gamma_3 = k a_3 \cos \theta + \alpha_3 \quad (21)$$

so that three geometric progressions can be identified as follows.

$$f_s = \sum_{j_s=0}^{n_s-1} e^{-i j_s \gamma_s}; \quad (s = 1, 2, 3). \quad (n_s \geq 1). \quad (22)$$

The series does not converge in general, but for a finite number of terms,

$$f_s = e^0 + e^{-i \gamma_s} + e^{-i 2 \gamma_s} + \dots + e^{-i (n_s - 1) \gamma_s}$$

and

$$(f_s e^{-i\gamma_s}) = e^{-i\gamma_s} + e^{-i2\gamma_s} + \dots + e^{-i(n_s)\gamma_s},$$

therefore,

$$f_s - f_s e^{-i\gamma_s} = 1 - e^{-in_s\gamma_s}$$

so that a closed-form expression can be employed for the uniform array such that

$$f_s = \frac{1 - e^{-in_s\gamma_s}}{1 - e^{-i\gamma_s}} = \frac{e^{-in_s\gamma_s/2}}{e^{-i\gamma_s/2}} \frac{\sin\left(\frac{n_s\gamma_s}{2}\right)}{\sin\left(\frac{\gamma_s}{2}\right)} = \frac{e^{-i(n_s-1)\gamma_s/2} \sin(n_s\gamma_s/2)}{\sin(\gamma_s/2)} \quad (23)$$

(s = 1, 2, 3)

Equation (14) can now be rewritten as

$$E = -i60 I_0 F'_0(\theta) \frac{e^{-i\xi}}{R} e^{-i(\delta_1 + \delta_2 + \delta_3)} f_1 f_2 f_3 e^{ikR - i\omega t} \quad (24)$$

This equation is sufficient to map all patterns for three-dimensional uniform arrays.

The collection  $f_1, f_2, f_3$  constitutes the lattice factors of the array and the magnitude of these factors (eq. 16, 17, 18) is  $F_1, F_2, F_3$  respectively. Since the lattice factors are associated with the amplitude or field intensity patterns in subsequent work, it is useful to determine the maximum value of each  $F_1, F_2, F_3$  and the least upper bound (supremum) of  $F_1 F_2 F_3$ .

$$F_s = |f_s| = \left| \frac{\sin(n_s\gamma_s/2)}{\sin(\gamma_s/2)} e^{-i(n_s-1)\gamma_s/2} \right| \quad (25)$$

(s = 1, 2, 3)

which is indeterminate for

$$\gamma_s/2 = 0, \pm\pi, \pm2\pi, \dots, (h_s\pi)$$



where  $h_s =$  any integer.

$$\lim_{\gamma_s/2 \rightarrow h_s \pi} \left| \frac{\sin(n_s \gamma_s/2)}{\sin(\gamma_s/2)} \right| = \lim_{\gamma_s/2 \rightarrow h_s \pi} \left| \frac{n_s/2 \cos(n_s \gamma_s/2)}{1/2 \cos(\gamma_s/2)} \right| = n_s. \quad (26)$$

The maxima of the lattice factors are therefore given by  $n_1, n_2, n_3$  corresponding to  $f_1, f_2, f_3$  respectively, and the least upper bound for the summation of component fields occurs when  $F_1 F_2 F_3 = n_1 n_2 n_3$ . This condition, simultaneous maxima for  $F_1, F_2, F_3$  is not a prerequisite for obtaining a principal beam maximum. That is,  $E$  (principal beam)  $\leq E$  (supremum) in general.

The function  $\sin(n_s \gamma_s/2)/\sin(\gamma_s/2)$  can be positive or negative, depending on the arguments  $(n_s \gamma_s/2)$  and  $(\gamma_s/2)$ , and is of considerable interest in general array studies. A plot of the numerator, denominator, quotient (field pattern) and quotient-squared (power pattern) is shown in Figure 3. Particular significance attaches to the sign of this function, or more precisely, the sign of the product of three such functions without the exponentials  $e^{-i(n_s-1)\gamma_s/2}$  ( $s = 1, 2, 3$ ). It is shown later in this report that the summation of simultaneously formed beams ultimately depends upon the sign of the triple product of lattice factors for each beam taken into a sum via the field superposition theorem. A detailed discussion of this, including the removal of the exponential terms  $e^{-i(n_s-1)\gamma_s/2}, e^{-i\xi}$  arising from the lattice factors and the source elements, respectively, is deferred to the discussion of scattering matrix gradients and beam summation.

#### ARRAY GAIN

An approximation to the maximum array gain can be made from Eq. (24), based on the principle of field superposition, if it is assumed that each of the  $n_2 n_3$  real (physically energized) sources dissipates as much energy when in

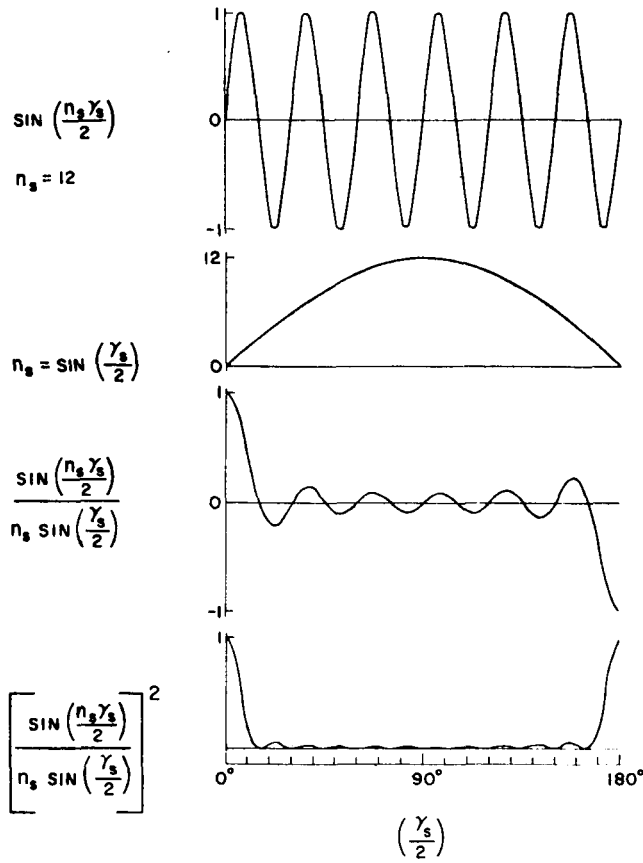


Figure 3-Composition and behavior of the  $\frac{1}{n_s} \frac{\sin\left(n_s \frac{\gamma_s}{2}\right)}{\sin\left(\frac{\gamma_s}{2}\right)}$  pattern function.

array over a perfect ground plane ( $n_1 = 2$ ) as when placed in a free-space environment. For definiteness half-wave dipoles are selected as source elements.

The general expression for antenna gain<sup>6</sup> is

$$G = \frac{P(\theta, \phi)}{\frac{1}{4\pi} \int_{\phi=0}^{2\pi} \int_{\theta=0}^{\pi} P(\theta, \phi) \sin \theta d\theta d\phi} \quad (27)$$

relative to a hypothetical isotropic radiator, from which the power gain of a half-wave dipole in free space is

$$G_{\lambda/2} = \frac{(F_0)^2}{\frac{1}{4\pi} \int_{\phi=0}^{2\pi} \int_{\theta=0}^{\pi} (F_0)^2 \sin \theta d\theta d\phi} \quad (28)$$

where

$$F_0 = \cos \left( \frac{\pi}{2} \cos \theta \right) / \sin \theta$$

$$\int_{\phi=0}^{2\pi} \int_{\theta=0}^{\pi} (F_0)^2 \sin \theta d\theta d\phi = \mathcal{E} = \frac{4\pi}{1.65} \quad (29)$$

is the total energy radiated from a single  $\lambda/2$  dipole. The validity of (29) follows from

$$G_{\lambda/2(\max.)} = \frac{1^2}{\frac{1}{4\pi} \left( \frac{4\pi}{1.65} \right)} = 1.65$$

which implies 2.17 db gain, a well-known value. The total energy  $\mathcal{E}_T$  from  $n_2 n_3$  dipoles of equal illumination is

$$\mathcal{E}_T \cong n_2 n_3 \left( \frac{4\pi}{1.65} \right) \quad (30)$$

which represents the total energy from the array by assumption. Then the array gain is

$$G_A \cong \frac{(F_0 F_1 F_2 F_3)^2}{\frac{1}{4\pi} \left[ n_2 n_3 \left( \frac{4\pi}{1.65} \right) \right]} \cong \frac{1.65 (F_0 F_1 F_2 F_3)^2}{n_2 n_3}.$$

The least upper bound (supremum) for all possible values of  $G_A$  is obtained for  $F_0 = 1$ ,  $F_1 = 2$ ,  $F_2 = n_2$ ,  $F_3 = n_3$ .

$$G_{A(\sup)} = (4) (1.65) n_2 n_3$$

$$G_{A(\sup)\text{db}} = 6.02 \text{ db.} + 2.18 \text{ db.} + 10 \log_{10} n_2 n_3 \text{ db.}$$

By way of example, for a square array of 256 elements,  $n_2 n_3 = 256$  and with  $a_2 = a_3 = \lambda/2$  say,

$$G_{16 \times 16}^{(\sup)} \text{ db} \cong 8.19 + 10 \log_{10} 256 \cong 32 \text{ db.}$$

Actually, the total power radiated from a collection of oscillators in array carrying an illumination  $I_{oj}$  is not, in general, equal to the totality of real oscillators times the power radiated from one such oscillator with the same illumination when the latter is considered separately.<sup>7</sup> Since Maxwell's equations are linear the superposition of fields is always admissible, but (1) addition of the Poynting vector ( $\vec{P} = \vec{E} \times \vec{H}$ ) or (2) addition of source element power, pertain to nonlinear combinations and are incorrect solutions for total power except in a few very special cases. It has been pointed out by Stone<sup>7</sup> and others that a pair of atoms radiate independently for a phase gradient  $\alpha_3 = \pi/2$ , separation  $a_3$  arbitrary and behave almost independently for  $\alpha = 0$ ,  $\alpha = \pi$  if  $a_3 > 0.7\lambda$ . These special cases have microwave analogues in a pair of identical linear and collinear antennas.

In general, the comparison of diffraction patterns should be predicated upon equal input power. This can be accomplished by (1) deriving the shape  $E = (F_0 F_1 F_2 F_3)$  of the patterns by means of the diffraction analysis, (2) forming the Poynting vector ( $\vec{P} = \vec{E} \times \vec{H}$ ), (3) determining the total radiation ( $\mathcal{E}_1 = \int_s P_s \sin\theta d\theta d\phi = K \int_s E_1^2 ds$ ) and (4) normalizing the patterns with respect to total power in each ( $\mathcal{E}_2 = K \int_s (\sqrt{C_0} E_2)^2 dS$ , where  $\mathcal{E}_1 = C_0 \mathcal{E}_2$  relates the total power in each pattern). The field patterns can then be weighted by  $\sqrt{C_0}$  which allows pattern comparison on an absolute basis. The subject of directive gain is presently being investigated with the assistance of an IBM 7090 computer to approximate the integral of Eq. (27) for various arrays under different conditions. The effect of element spacing, aperture gradients, and beam addition on antenna gain will be determined on an individual basis in subsequent reports for several array configurations.

## VON LAUE EQUATIONS

An appreciable amount of information can now be derived from the crystal lattice notation including (1) position of principal beam maxima, (2) grating lobe information, and (3) spurious beam information. Returning to Eq. (26), the indeterminacy leading to the realization of the maximum value for each lattice factor is identified by

$$\sin \gamma_s / 2 = 0 \quad (31)$$

which occurs when  $\gamma_s / 2 = h_s \pi$  if  $h_s$  equals an integer (plus, minus, or zero).

Then, from Eq. (19), (20), (21);

$$\gamma_1 = ka_1 \sin \theta \cos \phi + \alpha_1 = 2\pi h_1$$

$$\gamma_2 = ka_2 \sin \theta \sin \phi + \alpha_2 = 2\pi h_2$$

$$\gamma_3 = ka_3 \cos \theta + \alpha_3 = 2\pi h_3$$

or

$$\sin \theta \cos \phi = \left( h_1 - \frac{\alpha_1}{2\pi} \right) \frac{\lambda}{a_1} = u_1 \quad (32)$$

$$\sin \theta \sin \phi = \left( h_2 - \frac{\alpha_2}{2\pi} \right) \frac{\lambda}{a_2} = u_2 \quad (33)$$

$$\cos \theta = \left( h_3 - \frac{\alpha_3}{2\pi} \right) \frac{\lambda}{a_3} = u_3 \quad (34)$$

Equations (32), (33), (34) are the array analogues to the equations obtained by Max von Laue<sup>8</sup> for crystal diffraction maxima. These conditions are not necessarily satisfied simultaneously by any choice of  $\theta$  and  $\phi$  coordinate angles for arbitrarily chosen  $h_1, h_2, h_3$ . The choice of the lattice spacing and the array gradients determines the possibility of simultaneous solution of these equations.

A few simple examples illustrate the usefulness of the von Laue type equations. An array of elements which forms images by means of a perfectly conducting ground plane introduces a specific  $n_s$  and a specific  $\alpha_s$ . If the plane of the array is taken to be the y-z plane, then  $n_1 = 2$  and  $\alpha_1 = \pi$  for source elements oriented parallel to the y-z plane due to boundary conditions at the ground plane. Simultaneous solution of Eq. (32), Eq. (33), and Eq. (34) yields

$$1 = u_1^2 + u_2^2 + u_3^2 = \left[ \left( h_1 - \frac{\alpha_1}{2\pi} \right) \frac{\lambda}{a_1} \right]^2 + \left[ \left( h_2 - \frac{\alpha_2}{2\pi} \right) \frac{\lambda}{a_2} \right]^2 + \left[ \left( h_3 - \frac{\alpha_3}{2\pi} \right) \frac{\lambda}{a_3} \right]^2 \quad (35)$$

If  $a_1 = a_2 = a_3 = \lambda/2$  is arbitrarily selected for the array with source elements over the ground plane, then  $0 \leq \theta \leq \pi$ ,  $-\pi/2 \leq \phi \leq +\pi/2$  for physically realizable beams and

$$1 = (2h_1 - 1)^2 + \left( 2h_2 - \frac{\alpha_2}{\pi} \right)^2 + \left( 2h_3 - \frac{\alpha_3}{\pi} \right)^2. \quad (36)$$

The first term of Eq. (36) is minimized for  $h_1 = +1$  or  $h_1 = 0$ , the latter value being non-realizable for the array and ground-plane combination here since the beam forms in the physically inaccessible half-space. Then

$$1 = 1 + \left( 2h_2 - \frac{\alpha_2}{\pi} \right)^2 + \left( 2h_3 - \frac{\alpha_3}{\pi} \right)^2. \quad (37)$$

The two parenthetical terms must vanish if Eq. (37) is to be satisfied. If  $\alpha_2 = \alpha_3 = 0$  is imposed on the array there exists  $h_2 = h_3 = 0$  such that equality holds. If  $\alpha_2 = \alpha_3 = \pi/16$  is imposed on the array there does not exist any such combination of  $h_2$  and  $h_3$  and inequality holds for Eq. (37)

Since  $\alpha_2$  and  $\alpha_3$  are the gradients ordinarily associated with beam scanning, for the assumed array orientation, it is desirable that these parameters take on

many values besides  $0, \pm\pi, \pm 2\pi$ , etc. It is apparent that Eq. (35) cannot be satisfied for all choices of  $a_1, a_2, a_3$  and  $\alpha_1, \alpha_2, \alpha_3$ . The factor  $F_0 f_1$  in Eq. (24) can be regarded as the pattern resulting from the free-space source element  $F'_0$  and the influence of the ground plane  $f_1$ , so that the array problem reduces to a study of finding simultaneous solutions to Eq. (33) and Eq. (34) only. That is, a field point  $P(\theta, \phi)$  is to be located such that the maximum values  $F_{2_m} = |f_{2_m}| = n_2$  and  $F_{3_m} = |f_{3_m}| = n_3$  are to be brought into coincidence at some coordinate point  $P(\theta, \phi)$  and a value  $F_1 = |f_1| < F_{1_m} = n_1$ , will be accepted.  $F_1 < F_{1_m}$  implies that the beam principal maximum, if it exists, will be less than the least upper bound (supremum) of all the possible values of  $E$  attainable under free choice of  $a_1, a_2, a_3$  and  $\alpha_1, \alpha_2, \alpha_3$ .

Simultaneous solution of Eq. (33) and Eq. (34) yields

$$\cos \theta = u_3 = \left( h_3 - \frac{\alpha_3}{2\pi} \right) \frac{\lambda}{a_3} \quad (38)$$

$$\sin \phi = \frac{u_2}{(1 - u_3^2)^{1/2}} = \frac{\left[ \left( h_2 - \frac{\alpha_2}{2\pi} \right) \frac{\lambda}{a_2} \right]}{\left\{ 1 - \left[ \left( h_3 - \frac{\alpha_3}{2\pi} \right) \frac{\lambda}{a_3} \right]^2 \right\}^{1/2}} \quad (39)$$

under  $0 \leq \theta \leq \pi, 0 \leq \phi \leq 2\pi$

which provides the angular coordinates  $(\theta, \phi)$  if they exist.

Three simple examples are given to illustrate the significance of Eq. (38) and Eq. (39) in relation to normal (ordinary) beams, grating lobes, and spurious beams. (See Figure 2.)

### Example (I)

Let  $\alpha_1 = \pi$ ,  $a_1 = a_2 = a_3 = \lambda/2$  and  $0 \leq \theta \leq \pi/2$ ,  $-\pi/2 \leq \phi \leq +\pi/2$   
 $\alpha_2 = \alpha_3 = \pi/16$  is imposed.  
 $h_2 = h_3 = 0$  are unique possibilities.

One principal maximum forms, subject to  $F_0 F_1$ . This is an example of a "normal" beam. The array is over a perfectly conducting ground plane, the separation between all real and image oscillators is  $\lambda/2$ , and equal gradients are imposed in the (y) and (z) directions. The beam is "normal" in the sense that it is one of set of beams ordinarily formed by means of scattering matrices which generate gradients  $\alpha_2 = u\pi/n_2$  and  $\alpha_3 = v\pi/n_3$ , where u and v are odd integers. "Normal" or "orthogonal" beams as they are sometimes called have the characteristic that the principal maximum of one beam coincides in space with the minimum of an adjacent beam.

### Example (II)

Let  $\alpha_1 = \pi$ ,  $a_1 = a_2 = a_3 = \lambda$  and  $0 \leq \theta \leq \pi/2$ ,  $-\pi/2 \leq \phi \leq +\pi/2$   
 $\alpha_2 = \pi/16$ ,  $\alpha_3 = 13\pi/16$  is imposed.  
 $h_3 = 0$ ,  $h_3 = +1$ ,  $h_2 = 0$  are unique possibilities.

Two principal maxima form, subject to  $F_0 F_1$ . In this case a so-called "grating lobe" forms, but the principal maximum does not coincide with the grating lobe maximum in space. The array is over a perfectly conducting ground plane, the separation between all real and image oscillators is  $\lambda$  and unequal phase gradients are imposed in the (y) and (z) directions. In this instance the



increased element spacing allows the formation of grating lobes, if  $\alpha_2$  or  $\alpha_3$  are made sufficiently large. Grating lobes exhibit intensities which are equal to or less than the principal maxima for an array unless the source pattern  $F_0$  and the lattice factor  $F_1$  associated with it diminish the product  $F_0 F_1 F_2 F_3$  as is the case for large steering angles. Figure 4 illustrates typical linear grating lobe formation after  $F_0 F_1$  is allowed to operate on the factor  $F_3$ .  $F_2 = 1$  for a linear array here.

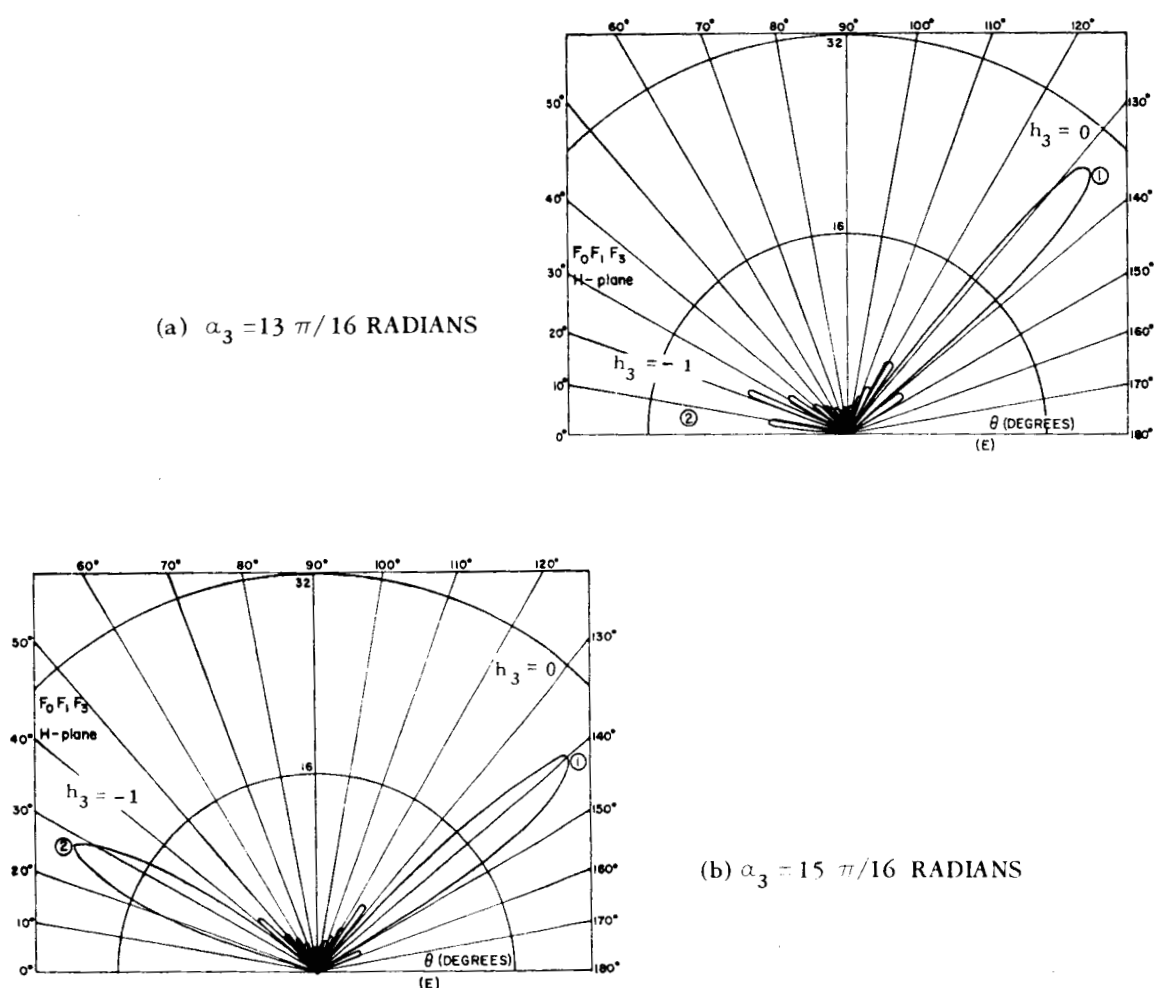


Figure 4-Principal maximum ①, and grating lobe ②, of linear array over ground-plane;  
 $a_1 = \lambda/2$ ,  $a_3 = 6 \lambda/10$ , and  $\lambda/2$  dipole source elements.

### Example (III)

Let  $\alpha_1 = \pi$ .  $a_1 = a_2 = a_3 = \lambda/2$

$\alpha_2 = \alpha_3 = 15\pi/16$   $0 \leq \theta \leq \pi$ ,  $-\pi/2 \leq \phi \leq +\pi/2$  is imposed.

A pair  $h_2, h_3$  does not exist. "Spurious beams" result instead of principal maxima, subject to  $F_0 F_1$ . The array is the same as in the first example, except that the phase gradients are larger. In this instance there does not exist a point in space such that the maximum value of the product  $F_2 F_3$  is realized. That is, the last two von Laue equations, Eq. (33) and Eq. (34), cannot be solved simultaneously for any given direction in space. This is sometimes referred to as "spurious" beam formation.

The von Laue type equations lead to a precise determination of the angular coordinates  $(\theta, \phi)$  of the beam principal maxima where  $F_0 F_1$  is isotropic only, a condition which is approached quite closely for many choices of source elements if the beam is not steered too far from the normal to the plane of the array. Ordinarily the exact field patterns are determined by evaluating  $F_0 F_1 F_2 F_3$ , but it is useful to retain the hypothetical isotropic sources here and elsewhere to obtain an insight of the function of the lattice factors  $F_2 F_3$  without the effects of the  $F_0 F_1$  term.

The lattice notation requires knowledge of the free-space pattern  $F_0$  only, and the effect of the ground plane is introduced by including the term  $F_1$ . As a specific example, the field of a single thin linear center-fed dipole in free space is given by<sup>9</sup>

$$E_\theta = \frac{i 60 |I_0|}{R} \left[ \frac{\cos\left(\frac{\pi L}{\lambda} \cos \theta\right) - \cos\left(\frac{\pi L}{\lambda}\right)}{\sin \theta} \right] \quad (40)$$

where  $L$  is the total dipole length. For the special case where  $L = \lambda/2$  Eq. (40) reduces to

$$\mathbf{E}_\theta = \frac{i 60 |\mathbf{I}_0|}{R} \left[ \frac{\cos \left( \frac{\pi}{2} \cos \theta \right)}{\sin \theta} \right] \quad (41)$$

Equation (41) corresponds to  $\mathbf{F}_0$  in the lattice notation and is therefore sufficient to describe this particular source element. It can easily be verified that

$$\left[ \frac{\cos \left( \frac{\pi}{2} \cos \theta \right)}{\sin \theta} \right] \mathbf{F}_1 = \mathbf{F}_0 \mathbf{F}_1 \quad (42)$$

leads to the same three-dimensional radiation pattern as the more complex expression<sup>10</sup>

$$\mathbf{F}_0 \mathbf{F}_1 = \mathbf{E}_\theta = j \left( \frac{\mu}{\epsilon} \right)^{1/2} \frac{\mathbf{I}_0 e^{-j[kR + (\psi/2)]}}{\pi R} \left[ \frac{\cos \left( \frac{\pi}{2} \cos \theta \right)}{\sin \theta} \right] \left[ \cos \left( \frac{\pi a}{\lambda} \sin \theta \sin \phi - \frac{\psi}{2} \right) \right] \quad (43)$$

where the following correspondences can be made between the notation of Silver and Stratton.

Silver	Stratton	Value
$j$	$i$	$\sqrt{-1}$
$e^{-jkR}$	$e^{+jkR}$	—
$\psi$	$\alpha_1$	$\pi$
$a$	$a_1$	—

Equation (43) holds for the half-wave dipole a distance  $a_1/2$  above a perfectly conducting ground plane and parallel to it. The relative ease with which source patterns can be developed, and the fact that the size or extent of the array does not increase the computational effort required to evaluate the lattice factors makes the lattice notation especially attractive.\*

---

\*The free-space source factor  $\mathbf{F}_0$  for a pair of crossed dipoles in arbitrary phase relationship is given in the Appendix A.

# BEAM MAXIMA, MINIMA, AND CROSSOVER LEVELS UNDER ORTHOGONALITY CONDITIONS

An examination of the function  $\sin(n_s \gamma_s/2)/\sin(\gamma_s/2)$ , as it appears in Eq. (23) and Eq. (24), leads to a set of equations for determining the beam nulls of a planar array. The procedure is similar to that for determining beam maxima by von Laue type equations. It is sufficient, however, for any one of  $F_0$ ,  $F_1$ ,  $F_2$ ,  $F_3$ , to vanish to establish a radiation pattern null or zero value for the field intensity.

$$f_1 = F_1 = \frac{\sin \frac{n_1}{2} (k a_1 \sin \theta \cos \phi + \alpha_1)}{\sin \frac{1}{2} (k a_1 \sin \theta \cos \phi + \alpha_1)} = 0 \quad (44)$$

if

$$\frac{n_1}{2} (k a_1 \sin \theta \cos \phi + \alpha_1) = \ell_1 \pi \quad (45)$$

where  $\ell_1$  belongs to the set of all integers ( $\ell_1 \in \mathbb{Z}$ ). Then

$$\sin \theta \cos \phi = \frac{\lambda}{a_1} \left( \frac{\ell_1}{n_1} - \frac{\alpha_1}{2\pi} \right) \quad (46)$$

with the restriction  $\ell_1 \neq n_1 h_1$  since  $\ell_1 = n_1 h_1$  leads to a maximum value for the lattice factor  $F_1$ . That is, Eq. (46) becomes Eq. (32).

Similarly,

$$f_2 = F_2 = \frac{\sin \frac{n_2}{2} (k a_2 \sin \theta \sin \phi + \alpha_2)}{\sin \frac{1}{2} (k a_2 \sin \theta \sin \phi + \alpha_2)} = 0 \quad (47)$$

if

$$\frac{n_2}{2} (k a_2 \sin \theta \sin \phi + \alpha_2) = \ell_2 \pi; \quad (\ell_2 \in \mathbb{Z}).$$

Then

$$\sin \phi = \frac{\lambda}{a_2 \sin \theta} \left( \frac{\ell_2}{n_2} - \frac{a_2}{2\pi} \right); \quad \ell_2 \neq n_2 h_2. \quad (48)$$

Similarly,

$$f_3 = F_3 = \frac{\sin \frac{n_3}{2} (k a_3 \cos \theta + \alpha_3)}{\sin \frac{1}{2} (k a_3 \cos \theta + \alpha_3)} = 0 \quad (49)$$

if

$$\frac{n_3}{2} (k a_3 \cos \theta + \alpha_3) = \ell_3 \pi; \quad (\ell_3 \in \mathbb{Z}).$$

Then

$$\cos \theta = \frac{\lambda}{a_3} \left( \frac{\ell_3}{n_3} - \frac{a_3}{2\pi} \right); \quad \ell_3 \neq n_3 h_3 \quad (50)$$

The usefulness of Eq. (46), Eq. (48), Eq. (50) can be demonstrated and some of the abstract character of these equations removed by an example. Assume an array over a ground plane such that arbitrarily chosen values are

$$n_1 = 2, \quad n_2 = 16, \quad n_3 = 16$$

$$a_1 = a_2 = a_3 = \lambda/2$$

$$\alpha_1 = \pi, \quad \alpha_2 = \frac{u\pi}{n_2}, \quad \alpha_3 = \frac{v\pi}{n_3}; \quad (u, v) \in (\mathbb{Z}_{\text{odd}}),$$

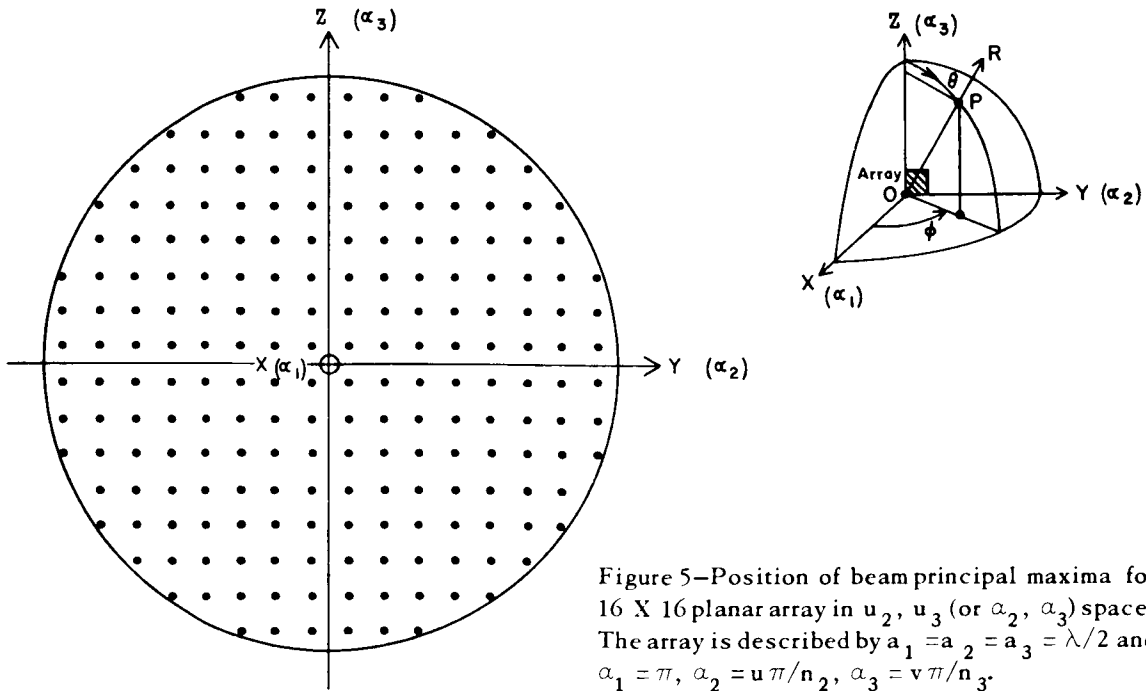
so that  $\alpha_2 = 1\pi/16, 3\pi/16, \dots, 15\pi/16$  and  $\alpha_3 = 1\pi/16, 3\pi/16, \dots, 15\pi/16$ .

Phase gradients given by the odd-integer rule above are physically realizable and lead to the concept of simultaneous orthogonal beams. A physical means for obtaining such gradients is presented later in this report under composite scattering matrices.

From Eq. (46);  $\ell_1 = n_1 h_1 = 0$  implies  $F_1 = F_1(\text{max})$  and  $h_1 = 0$ , but can be ignored for the half-space given by  $0 \leq \theta \leq \pi$  and  $-\pi/2 \leq \phi \leq +\pi/2$ .  $\ell_1 = +1$

implies that there exists an infinity of zeros corresponding to  $\phi = +\pi/2$ ,  $0 \leq \theta \leq \pi$  and  $\phi = -\pi/2$ ,  $0 \leq \theta \leq \pi$ .  $\ell_1 = +2 = n_1 h_1$  implies  $F = F_1$  (max) and  $h_1 = +1$  which is in the physically accessible half-space.  $\ell_1 > 2$  and  $\ell_1 < 0$  will not satisfy Eq. (46) and can be ignored. This exhausts all possible choices of  $\ell_1$  and formally establishes the fact that the lattice factor  $F_1$  has only one physically realizable maximum for the assumed array. The infinity of zeros in the y-z plane ensures that the field intensity of the far-field pattern vanishes in the extended plane of the metallic boundary. The latter statement is independent of spacing  $a_1$  in Eq. (46) and is a consequence of  $n_1 = 2$ ,  $\alpha_1 = \pi$ .

A plot of the principle beam maxima positions for the assumed planar array appears as shown in Figure 5, and results from the use of the generally valid Eq. (38) and Eq. (39). The factor  $F_0 F_1$  can be ignored here if the source pattern is slowly varying with  $(\theta, \phi)$ .



$$u_3 = \cos \theta = \left( h_3 - \frac{\alpha_3}{2\pi} \right) \frac{\lambda}{a_3} \quad (38)$$

$$\frac{u_2}{(1 - u_3^2)^{1/2}} = \sin \phi = \frac{\left[ \left( h_2 - \frac{\alpha_2}{2\pi} \right) \lambda / \alpha_2 \right]}{\left\{ 1 - \left[ \left( h_3 - \frac{\alpha_3}{2\pi} \right) \lambda / \alpha_3 \right]^2 \right\}^{1/2}} \quad (39)$$

It appears from the plot of Figure 5 that the beams are equispaced in  $(u_2, u_3)$  space. This is shown by simple proof. Since the assumed array exhibits no grating lobes it follows that the unique values  $h_2 = h_3 = 0$  are associated with simultaneous maximum values of  $F_2 F_3$  if a beam principal maximum exists. The total number of principal maxima in the physically accessible half-space is seen to be 208 rather than  $n_2 n_3 = 256$ . Equations (33) and (34) cannot be solved for 48 combinations of  $(\alpha_2, \alpha_3)$  which lead to spurious beam formation.

Using

$$u_2 = \sin \theta \sin \phi = \left( h_2 - \frac{\alpha_2}{2\pi} \right) \frac{\lambda}{a_2}, \quad (33)$$

$$u_3 = \cos \theta = \left( h_3 - \frac{\alpha_3}{2\pi} \right) \frac{\lambda}{a_3}; \quad (34), (38)$$

$$u_2 = -\alpha_2 / \pi, \quad (51)$$

$$u_3 = -\alpha_3 / \pi. \quad (52)$$

Since  $\alpha_2 = u\pi/n_2$  and  $\alpha_3 = v\pi/n_3$  and  $n_2 = n_3$  here (square array), it follows that "adjacent" beam principal maxima are equispaced in  $(u_2, u_3)$  space and form a

perfectly square grid as shown in Figure 5. "Adjacent" implies  $\alpha_2$  is a constant, and  $\alpha_3$  is a variable or vice versa. The coordinate system of Figure 5 is developed graphically in Figure 6, where concentric circles in the  $y$ - $z$  plane are used to map space points associated with  $(\theta_1, \phi_1)$ ,  $(\theta_1, \phi_4)$ ,  $(\theta_1, \phi_{10})$  and  $(\theta_2, \phi_1)$ ,  $(\theta_2, \phi_4)$ ,  $(\theta_2, \phi_{10})$  or the  $u_2, u_3$  plane.

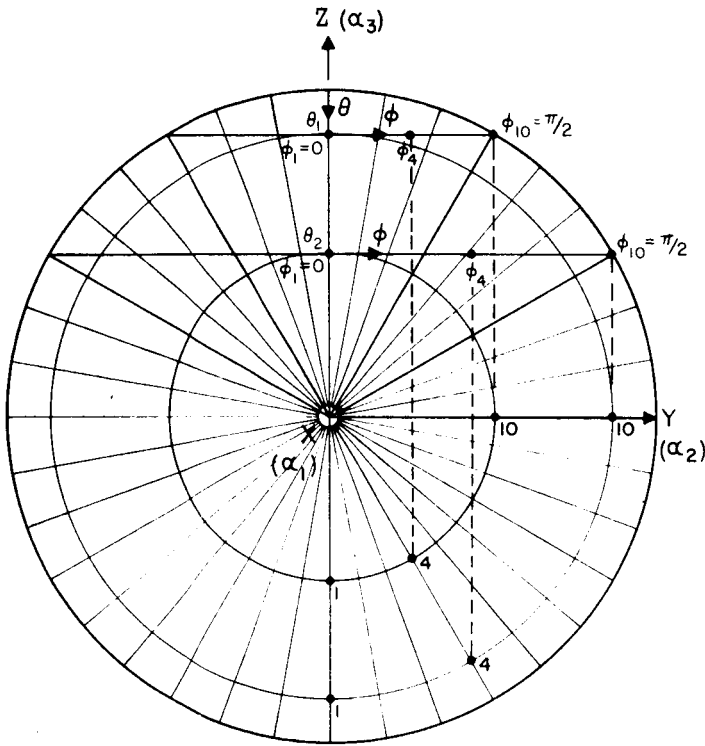


Figure 6—Development of coordinate system  $(u_2, u_3)$ .  $u_2 = \sin \theta \sin \phi$ ,  $u_3 = \cos \theta$ .

It is now relatively easy to show that the nulls of adjacent beams occur at common angles for orthogonal beams. From Eq. (48) and  $\alpha_2 = u\pi/n_2$ ,

$$\sin \phi = \frac{\lambda}{a_2 \sin \theta} \left( \frac{\ell_2}{n_2} - \frac{u}{2n_2} \right); \quad \ell_2 \neq n_2 h_2, \quad (53)$$

yields a zero for the field pattern. For any two adjacent beams generated by  $u$  and  $u + 2 = u'$  (odd integers) the following is possible:

$$\frac{\ell_2}{n_2} - \frac{u}{2n_2} = \frac{\ell'_2}{n_2} - \frac{u'}{2n_2}.$$



Then the primed and unprimed beams have a common zero when  $\ell'_2 = \ell_2 + 1$ . A similar argument can be presented using Eq. (50).

$$\cos \theta = \frac{\lambda}{a_3} \left( \frac{\ell_3}{n_3} - \frac{\alpha_3}{2\pi} \right); \quad \ell_3 \neq n_3 h_3. \quad (54)$$

Here  $\alpha_3 = v\pi/n_3$ , and  $v$  and  $v' = v + 2$  are used.

In the above  $(u, v) \in (z \text{ odd})$  as before.

It also follows that for adjacent orthogonal beams the principal maximum of any beam coincides with the nulls of all other beams. The proof is presented for Eq. (48) only since the same argument can be applied using Eq. (54). A beam maximum is implied by  $\ell_2 = 0$  for the unprimed beam which is generated by an aperture phase gradient  $(u)\pi/n_2$ . A minimum is implied by  $\ell'_2 = 1$  for the adjacent or primed beam generated by a  $(u + 2)\pi/n_2$  gradient. Then

$$\sin \phi = \frac{\lambda}{n_2 a_2 \sin \theta} \left( 0 - \frac{u}{2} \right) = \frac{\lambda}{n_2 a_2 \sin \theta} \left( 1 - \frac{u + 2}{2} \right)$$

and the proof is complete.

The angular position  $P(\theta, \phi)$  at which the principal maxima of adjacent orthogonal beams intersect can be found for the planar array using Eq. (24). Elimination of factors not relevant to the crossover level determination leaves

$$F_0 F_1 F_2 F_3 = F'_0 F'_1 F'_2 F'_3 \quad (55)$$

where  $F_0 = F'_0$ ,  $F_1 = F'_1$  at the point of crossover only, and  $F_3 = F'_3$  if the two beams are adjacent in the sense that  $\alpha_2 = u\pi/n_2$  and  $\alpha'_2 = (u + 2)\pi/n_2$  and  $\alpha_3 = \alpha'_3$ . The problem then reduces to

$$\left| \frac{\sin \left[ \frac{n_2}{2} (k a_2 \sin \theta \sin \phi + \alpha_2) \right]}{\sin \frac{1}{2} (k a_2 \sin \theta \sin \phi + \alpha_2)} \right| = \left| \frac{\sin \left[ \frac{n_2}{2} (k a_2 \sin \theta \sin \phi + \alpha'_2) \right]}{\sin \frac{1}{2} (k a_2 \sin \theta \sin \phi + \alpha'_2)} \right| \quad (56)$$

via Eq. (25).

The condition for a solution to Eq. (56) is that

$$(k a_2 \sin \theta \sin \phi + \alpha_2) = - (k a_2 \sin \theta \sin \phi + \alpha'_2) \quad (57)$$

which can be shown by the following. For small values of the argument ( $\gamma_s/2$ ) such as are encountered for beam intersections lying between the principal maxima and the first null,

$$\frac{\sin n_s \gamma_s / 2}{\sin \gamma_s / 2} = \frac{\sin n_s \gamma_s / 2}{\gamma_s / 2} = \frac{\sin n_2 (k a_2 \sin \theta \sin \phi + \alpha_2)}{(k a_2 \sin \theta \sin \phi + \alpha_2)}. \quad (58)$$

Let  $k a_2 \sin \theta \sin \phi = \chi$  and  $\alpha_2 > \alpha'_2$ . Then

$$f(\chi, \alpha_2) = \frac{\sin n_2 (\chi + \alpha_2)}{(\chi + \alpha_2)} \quad (59)$$

and

$$g(\chi, \alpha'_2) = \frac{\sin n_2 (\chi + \alpha'_2)}{(\chi + \alpha'_2)} \quad (60)$$

which are both even functions. It follows that

$$g(\chi, \alpha'_2) = f(\chi, \alpha_2) \quad (61)$$

at the point of intersection of adjacent beams. But Eq. (59) and Eq. (60) are even functions. Therefore, Eq. (61) is satisfied if

$$(\chi + \alpha_2) = (\chi + \alpha'_2) \quad (62)$$

or

$$(\chi + \alpha_2) = - (\chi + \alpha'_2). \quad (63)$$

Eq. (62) forces the conclusion that  $\alpha_2 = \alpha'_2$  which represents two beams everywhere coincident in space, and violates the assumption that  $\alpha_2 = u\pi/n_2$  and  $\alpha'_2 = (u+2)\pi/n_2$  for adjacent beams. From Eq. (63) it follows that  $2ka_2 \sin \theta \sin \phi_c = -(\alpha'_2 + \alpha_2)$ , which is the condition stated in Eq. (57). Rewriting,

$$\sin \phi_c = \frac{-(\alpha'_2 + \alpha_2)}{2ka_2 \sin \theta} = \frac{-\lambda(u+1)}{2n_2 a_2 \sin \theta} \quad (64)$$

where  $\phi_c$  is the value of  $\phi$  at crossover and  $u$  is the least value for the two beams selected. Similarly if  $\alpha_2 = \alpha'_2$ , but  $\alpha_3 \neq \alpha'_3$ ,

$$\cos \theta_c = \frac{-\lambda(v+1)}{2n_3 a_3} \quad (65)$$

where  $\theta_c$  is the value of  $\theta$  at crossover and  $v$  is the least value for the two beams selected.

The utility of Eq. (64) and Eq. (65) is illustrated by two examples.

Let  $u = -1$  and  $u' = -1+2$ ;  $\alpha_3 = \alpha'_3$ . Then the lesser of  $-1, +1$  is  $-1$  in Eq. (64).

$$\sin \phi_c = \frac{-\lambda(u+1)}{2n_2 a_2 \sin \theta} = 0 \quad \text{and} \quad \phi_c = 0.$$

Let  $v = -1$  and  $v' = -1+2$ ;  $\alpha_2 = \alpha'_2$ . Then the lesser of  $-1, +1$  is  $-1$  in Eq. (65).

$$\cos \theta_c = \frac{-\lambda(v+1)}{2n_3 a_3} = 0 \quad \text{and} \quad \theta_c = \pi/2.$$

If  $\phi_c$  is substituted into the expression for the lattice factor  $F_{2c}$ , Eq. (25) for  $s = 2$ , or if  $\theta_c$  is used to evaluate the lattice factor  $F_{3c}$ , Eq. (25) for  $s = 3$ , the following hold. Here  $n_2 \gg 1$  or  $n_3 \gg 1$ .

$$F_{2c} = 2n_2/\pi \quad (66)$$

$$F_{3c} = 2n_3/\pi \quad (67)$$

Assuming  $F_{0 \text{ prin. max.}} \approx F'_{0 \text{ prin. max.}}$  and  $F_{1 \text{ prin. max.}} \approx F'_{1 \text{ prin. max.}}$  for the adjacent beams it makes sense to state that the crossover level, referred to the main beam principal maxima, is given by

$$\frac{F_{2c}}{F_{2 \text{ prin. max.}}} = \frac{2n_2}{\pi n_2} = \frac{F_{3c}}{F_{3 \text{ prin. max.}}} = \frac{2n_3}{\pi n_3} = \frac{2}{\pi} \quad (68)$$

even if  $F_{0 \text{ prin. max.}} < 1$  and  $F_{1 \text{ prin. max.}} < 2$ .  $\xi_2 \approx \xi_{2c}$ ,  $\xi_3 \approx \xi_{3c}$ ;  $\sqrt{C_0} \approx 1$  implicitly.

That is, the crossover level is approximately 3.9 decibels below the beam principal maximum level under the special restrictions given above.

The preceding discussion, pertaining to adjacent beam crossover levels for planar arrays, holds equally well for linear arrays and either Eq. (64) or Eq. (65) can be made applicable by proper orientation of the linear array in the coordinate frame. A set of E-plane radiation patterns derived for a 16×1 (linear) array of half-wave dipoles is shown in Figure 7. The difficulty of defining the beam crossover levels for all steering angles in any simple manner is illustrated by the patterns with the largest beam-steering gradients.

## SIMPLE SCATTERING MATRICES

The subject of corporate feeds is extensive and will be limited here to a brief discussion of passive circuits composed of hybrid coupler elements. Even this restricted topic can lead to numerous involved discussions, therefore, the present development will be carried just far enough to allow several examples of the application of the crystal lattice notation given earlier. Since the basic components of beam-forming matrices are 3-db. directional couplers and hybrid rings, the mathematical representation of these components is given without derivation,

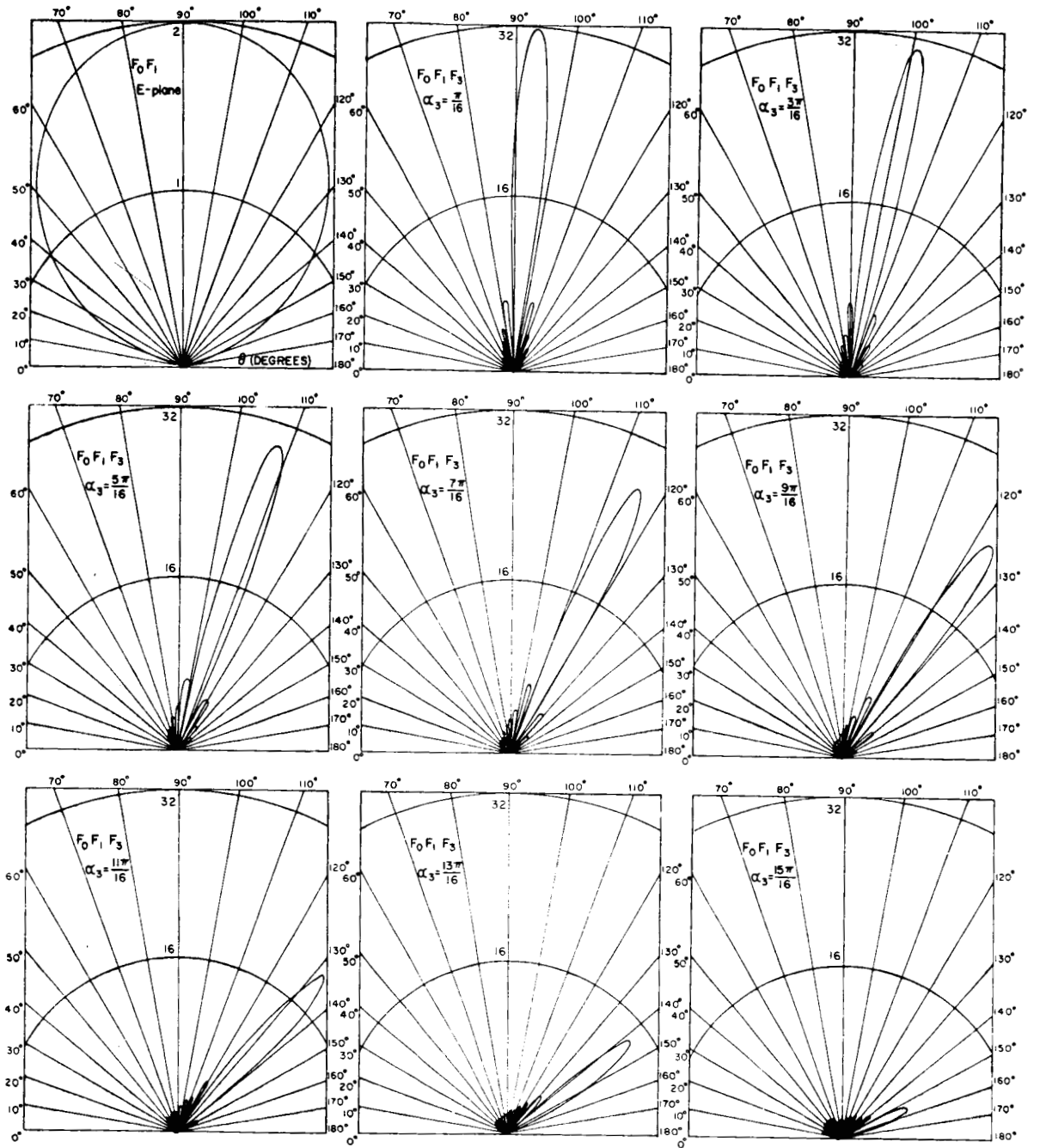


Figure 7-Adjacent beams of  $16 \times 1$  linear array of half-wave dipoles over ground-plane.  $a_1 = a_3 = \lambda/2$ ,  $\alpha_1 = \pi$ ,  $\alpha_3 = v\pi/16$

followed by one composite scattering matrix associated with antenna beam scanning circuitry.

Coupler and ring type "magic tees" are shown in Figure 8 together with their respective (coaxial) scattering matrices.<sup>12</sup> The convention adopted here is that only the angle  $\psi$ , say, will be entered as a matrix element of large matrices for a real time delay  $e^{-j\psi}$  where the context makes the meaning clear. A scattering matrix element is taken as the reflection or transmission coefficient between an input terminal (j) and an output terminal (i), where  $i, j$  is the row-column designation. Both  ${}_{\circ}S_{ij}$  and  ${}_{\square}S_{ij}$  are symmetric matrices since  $S_{ij} = S_{ji}$  and are in fact both unitary<sup>13</sup> matrices since the complex conjugate  $(S_{ij})^*$  transposed, or  $(S_{ij}^*)^t$ , times the original scattering matrix  $S_{ij}$  gives the identity matrix  $I$ , where  $I$  is a diagonal matrix with unit elements.

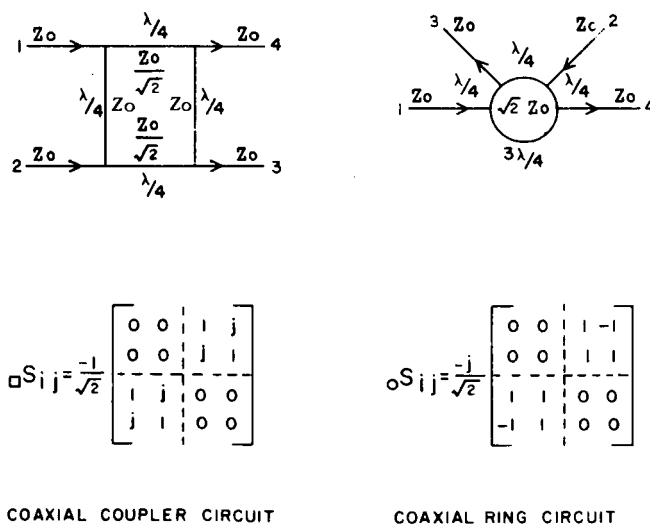


Figure 8-Magic T coaxial configurations and the associated scattering matrices.

Only the coupler type circuit will be employed in the remainder of this report, however, the equivalence of the ring and coupler types is formally established by the following transformation. The terminal (reference) planes of the four lines attached to the coupler circuit can be displaced by the transformation

$${}_{\square}S'_{ij} = P {}_{\square}S_{ij} P \quad (69)$$

where  $P$  is a diagonal matrix with elements  $P_{kk} = e^{-j\psi_k}$  corresponding to the  $k^{\text{th}}$  line into which a phase-shifting element is introduced. The choice of the  $\psi_k > 0$ , above is consistent with the use of a negative angle for a real time delay in the writing of the  $S_{ij}$  previously. If the two scattering matrices are equivalent,

$${}_oS_{ij} = {}_{\square}S'_{ij} = P {}_{\square}S_{ij} P \quad (70)$$

After premultiplication and postmultiplication of  ${}_{\square}S_{ij}$  by  $P$  the  ${}_{\square}S'_{ij}$  is compared to  ${}_oS_{ij}$  on an element-by-element basis, yielding the following equalities.

$$j = e^{-j(\psi_1 + \psi_3)} = e^{-j(\psi_2 + \psi_4)} \quad (71)$$

$$-1 = e^{-j(\psi_1 + \psi_4)} \quad (72)$$

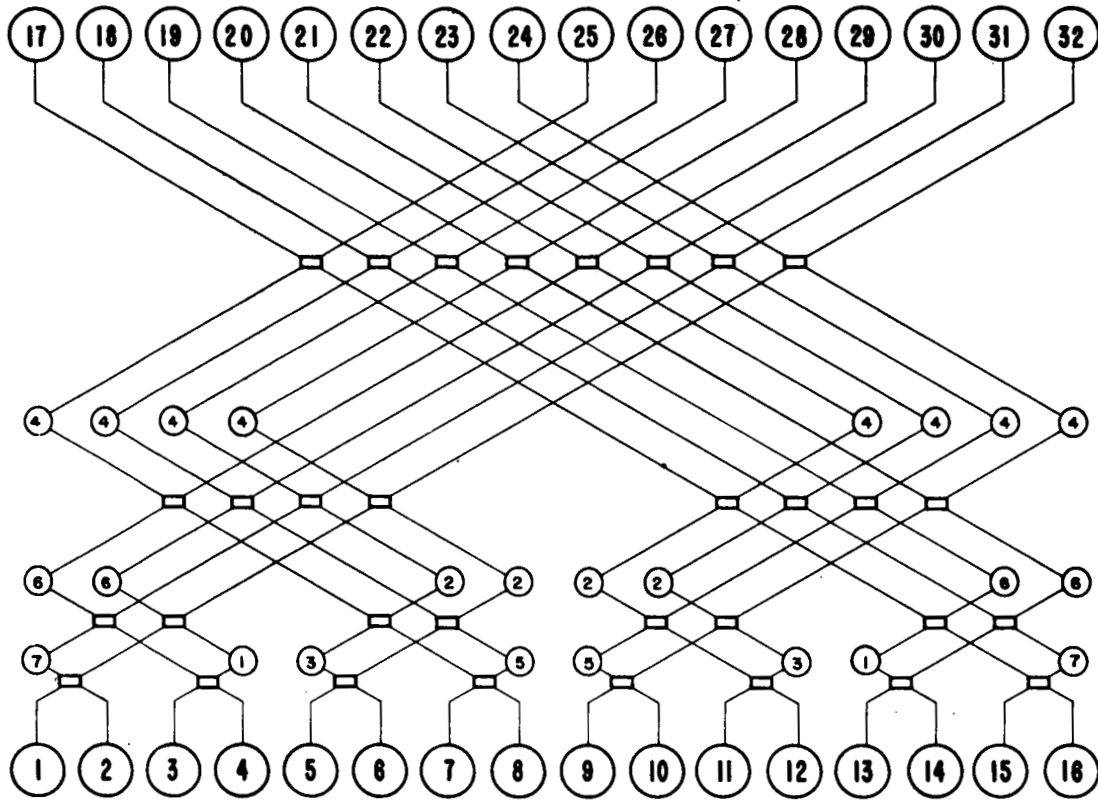
$$+1 = e^{-j(\psi_2 + \psi_4)} \quad (73)$$

Therefore  $\psi_1 = 0$ ,  $\psi_2 = \pi/2$ ,  $\psi_3 = 3\pi/2$ ,  $\psi_4 = \pi$ ,  $\psi_i \geq 0$  are solutions. Placement of corresponding delay lines in lines (1), (2), (3), (4) of the coupler circuit is required to make  ${}_oS_{ij}$  and  ${}_{\square}S_{ij}$  indistinguishable from one another.

## COMPOSITE SCATTERING MATRICES

The synthesis of composite scattering matrices for beam scanning will be deferred to a later report, but a typical circuit is presented as Figure 9. This

# ANTENNA PORTS



# BEAM PORTS

Figure 9-Simultaneous beam-forming matrix for  $16 \times 1$  (linear) array composed of coupler-type magic T elements and fixed phase shifters.

particular configuration forms 16 independent orthogonal beams, individually or simultaneously, and the associated scattering matrix  ${}_{16,1}S_{ij}$  is given as Eq. (74). Ordinarily a beam-forming matrix of this type is associated with linear antenna arrays.

$${}_{n_2, n_3}S_{ij} = {}_{16,1}S_{ij} = \frac{1}{4} \begin{bmatrix} A_{ij} & B_{ij} \\ C_{ij} & D_{ij} \end{bmatrix} \quad (74)$$



$S_{ij} = e^{-j\psi}$  in real time. Only the angle  $(+\psi)$  is entered as an element of the scattering matrix here, for compactness of writing and is expressed in units of  $\pi/n_2 = \pi/16$  since  $\alpha_2 = u\pi/n_2$  where  $u \in (z \text{ odd})$ . In Eq. (74), the partitions  $A_{ij}$  and  $D_{ij}$  of matrix  ${}_{16,1}S_{ij}$  are null, representing matched conditions at all ports and perfect isolation between input or output ports. Since  ${}_{16,1}S_{ij}$  is symmetric about the principal diagonal,  $B_{ij} = C_{ji}$ . These  $16 \times 16$  matrices are partitions of the  $32 \times 32$  matrix  ${}_{16,1}S_{ij}$ . Matrix  $C_{ij}$  is presented in complete detail in Figure 10. It is noted that  ${}_{16,1}S_{ij}$  is a unitary matrix. Since  $({}_{16,1}S_{ij}^*)^t ({}_{16,1}S_{ij}) = I$ .

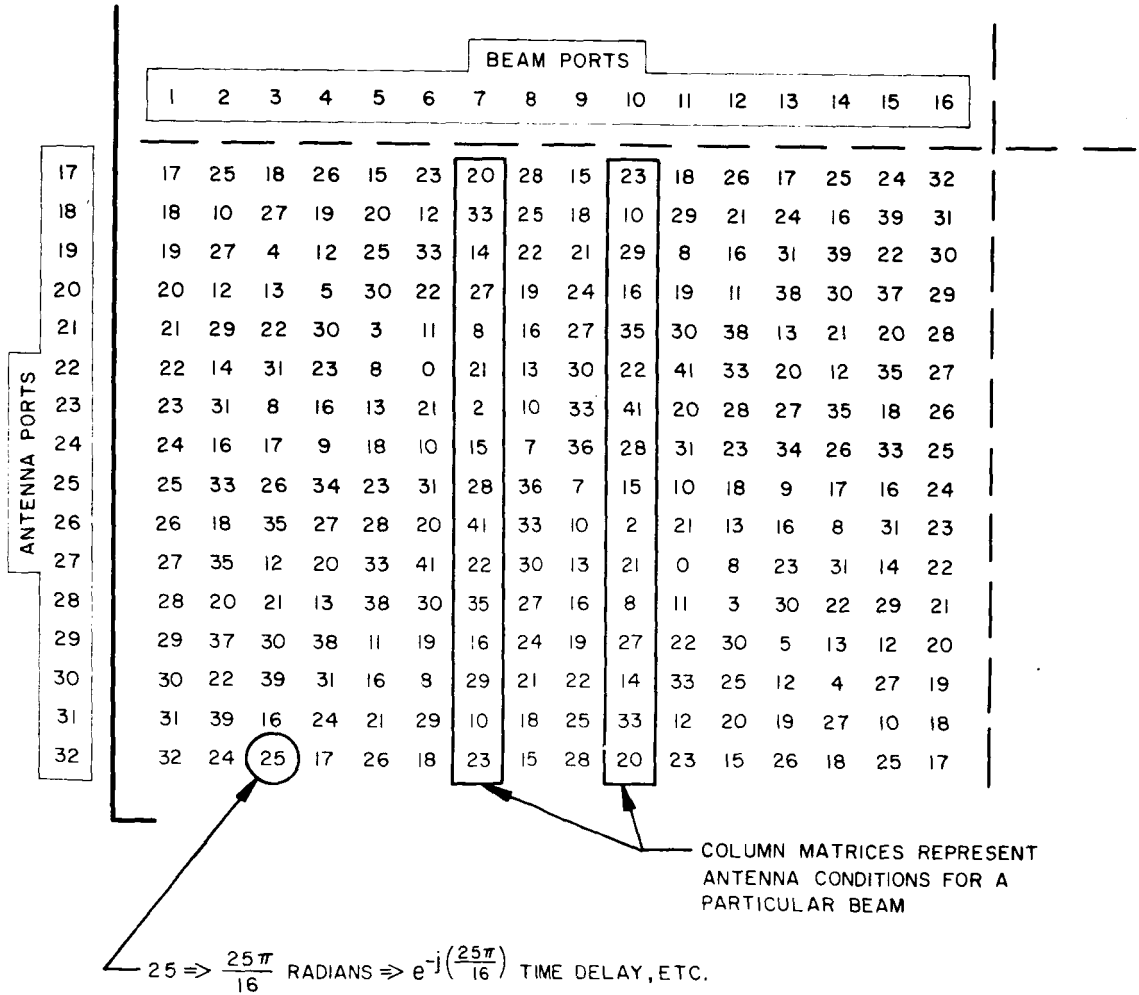


Figure 10-Partition  $C_{ij}$  of matrix  ${}_{16,1}S_{ij}$ .

In like manner the scattering matrices of planar arrays can be written. If  ${}_{16,1}S_{ij}$  is utilized as the basic component (matrix), the composite beam-forming circuit of Figure 11 results; the associated scattering matrix being

$${}_{n_2, n_3}S_{ij} = {}_{16,16}S_{ij} = \frac{1}{16} \begin{bmatrix} A_{ij} & B_{ij} \\ C_{ij} & D_{ij} \end{bmatrix} \quad (75)$$

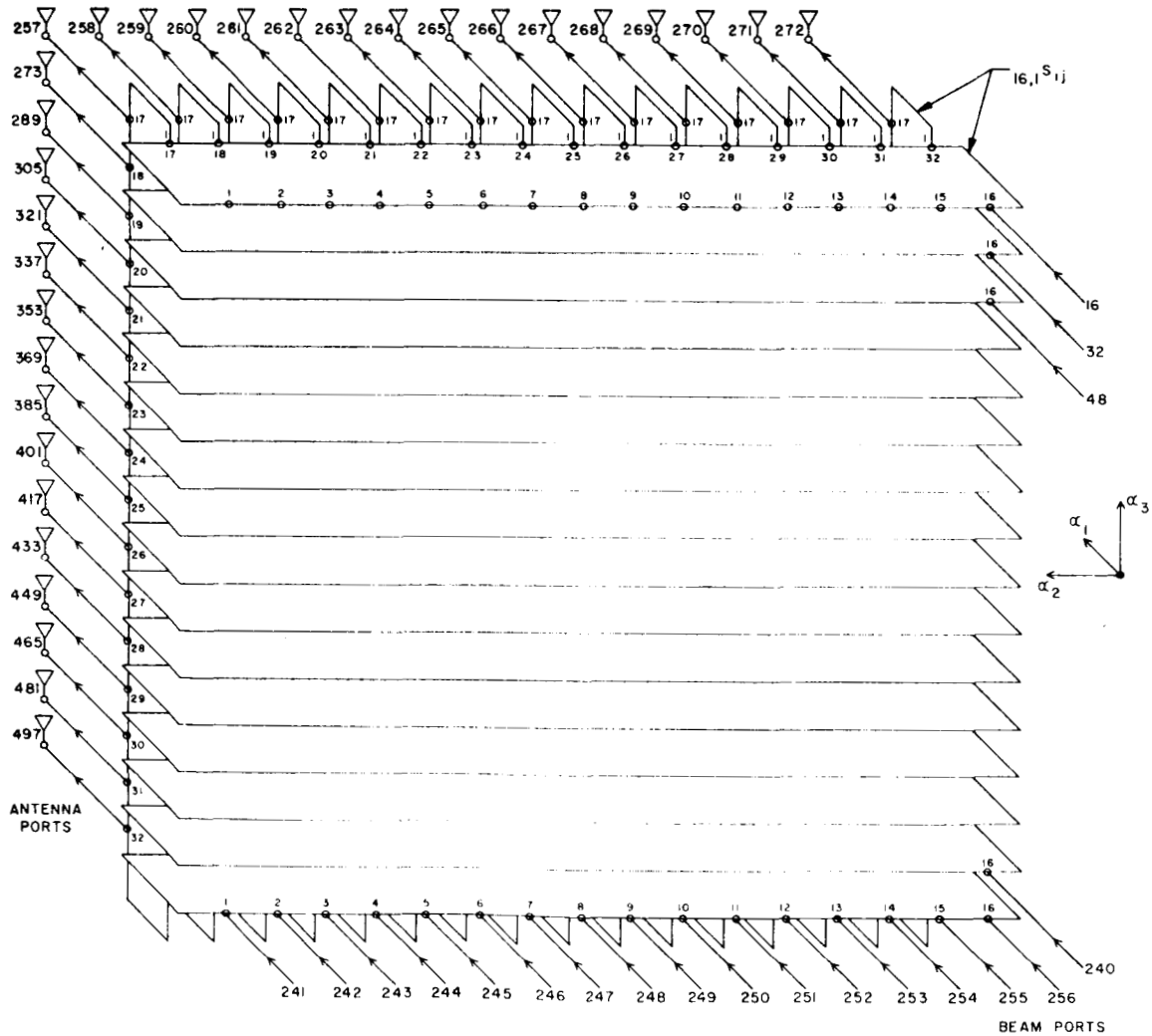
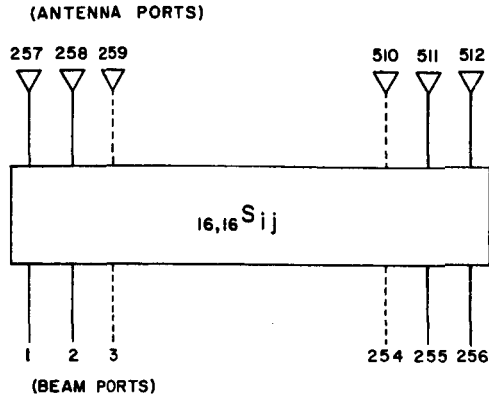


Figure 11—Composite beam-forming circuit utilizing thirty-two  ${}_{16,1}S_{ij}$  matrices.

where the  $A_{ij} = D_{ij} = 0$  as before. Here  $B_{ij}$  and  $C_{ij}$  are not the same as in Eq. (74) since now each of these partitions is a  $256 \times 256$  matrix of the overall  $512 \times 512$  matrix  ${}_{16,16}S_{ij}$ . Any column of  $C_{ij}$  represents the phase conditions on the aperture of a 256-element square array of antenna elements. Only  $C_{ij}$  is required to investigate various independent antenna beams, and  $B_{ij}$  can always be generated by the simple expedient of transposing the subscripts (ij) in  $C_{ij}$ . That is,  $B_{ij} = C_{ji}$  in general. If the antenna ports are used as beam ports the column matrices of  $B_{ij}$  determine the phase gradients across the antenna aperture. Equation (76) illustrates the manner in which the aperture gradients can be identified for the planar array of 256 radiators depicted in Figure 12. The space relationship among the radiators is not indicated here.

$${}_{16,16}S_{ij} = \frac{1}{16} \left[ \begin{array}{c|c} \begin{array}{c} A_{ij} \text{ (null)} \\ \hline C_{257,1} \quad C_{257,2} \text{---} C_{257,255} \quad C_{257,256} \\ C_{258,1} \quad C_{258,2} \text{---} C_{258,255} \quad C_{258,256} \\ \vdots \quad \vdots \quad \vdots \quad \vdots \\ C_{511,1} \quad C_{511,2} \text{---} C_{512,255} \quad C_{511,256} \\ C_{512,1} \quad C_{512,2} \text{---} C_{512,255} \quad C_{512,256} \end{array} & \begin{array}{c} B_{1,257} \quad B_{1,258} \text{---} B_{1,511} \quad B_{1,512} \\ B_{2,257} \quad B_{2,258} \text{---} B_{2,511} \quad B_{2,512} \\ \vdots \quad \vdots \quad \vdots \quad \vdots \\ B_{255,257} \quad B_{255,258} \text{---} B_{255,511} \quad B_{255,512} \\ B_{256,257} \quad B_{256,258} \text{---} B_{256,511} \quad B_{256,512} \end{array} \\ \hline & \begin{array}{c} D_{ij} \text{ (null)} \end{array} \end{array} \right] \quad (76)$$



$$\text{Number of beams} = N_B$$

$$\text{Number of hybrids} = N_H = \frac{1}{2} N_B \log_2 N_B$$

$$\text{Number of internal phase shifters} =$$

$$N_P = \frac{1}{2} N_B \left[ \left( \log_2 N_B \right) - 1 \right]$$

Figure 12—Schematic representation of scattering circuit for 256-element planar array of radiators.

Under the transposition  $B_{ij} = C_{ji}$ , the column matrix  $B_{i,257}$  corresponds to the aperture phase gradient when the antenna port 257 is used as a beam port, for example, and

$$\begin{bmatrix} B_{1,257} \\ B_{2,257} \\ \vdots \\ B_{255,257} \\ B_{256,257} \end{bmatrix} = \begin{bmatrix} C_{257,1} \\ C_{257,2} \\ \vdots \\ C_{257,255} \\ C_{257,256} \end{bmatrix} \quad (77)$$

The scattering matrix  $_{16,16}S_{ij}$  is symmetric since it is equal to its own transpose, but the antenna ports cannot be employed as beam ports. Nevertheless the  $_{16,16}S_{ij}$  matrix is reciprocal in the sense that either transmitting or receiving equipments can be utilized at the beam ports; a unique pattern exists for these two modes of operation. It is noted that the scattering matrices of simple coupler

and ring hybrids are both symmetric and unitary, as are the composite scattering matrices  ${}_{16,1}S_{ij}$  and  ${}_{16,16}S_{ij}$ .

## BEAM COMBINING

The possibility of weighted addition and subtraction of two or more of the independently formed beams derived from a planar aperture is now considered. Using the notation employed in the preceding analysis, the particular case of a  $16 \times 16$  element planar array is selected as an example and the composite beam-forming matrix of Figure 11 is utilized. Some attention must now be given to the absolute time delays involved in passing through the beam-forming matrix before performing any sum or difference operations. The beams are summed in space according to the superposition theorem discussed previously, therefore, Eq. (24) is repeated here for convenience,

$$E = - \frac{i 60 I_0 F'_0(\theta)}{R} e^{-i\xi} e^{-(\delta_1 + \delta_2 + \delta_3)} f_1 f_2 f_3 e^{ikR - i\omega t}. \quad (24)$$

The surface on which the fields are observed will be taken as the sphere of radius  $R$ ; all source elements are assumed to be identical; and the frequency of two simultaneously generated beams, A and B, is  $f_A = f_B = \omega / 2\pi$ .

The interference phenomena on the sphere of observation now depend on the interaction of two beams

$$E_A = k_A e^{-i(\delta_{1A} + \delta_{2A} + \delta_{3A})} f_{1A} f_{2A} f_{3A} \quad (78)$$

and

$$E_B = k_B e^{-i(\delta_{1B} + \delta_{2B} + \delta_{3B})} f_{1B} f_{2B} f_{3B}, \quad (79)$$

where  $k_A$  and  $k_B$  are constants of proportionality and equal or unequal weight

can be ascribed to these constants. By Eq. (23), the  $E_A$  and  $E_B$  above can be rewritten as

$$E_A = k_A e^{-i(\delta_{1A} + \delta_{2A} + \delta_{3A})} \frac{\sin n_1 \gamma_{1A}/2}{\sin \gamma_{1A}/2} \frac{\sin n_2 \gamma_{2A}/2}{\sin \gamma_{2A}/2} \frac{\sin n_3 \gamma_{3A}/2}{\sin \gamma_{3A}/2} e^{-i[(n_1 - 1)\gamma_{1A}/2 + (n_2 - 1)\gamma_{2A}/2 + (n_3 - 1)\gamma_{3A}/2]} \quad (80)$$

$$E_B = k_B e^{-i(\delta_{1B} + \delta_{2B} + \delta_{3B})} \frac{\sin n_1 \gamma_{1B}/2}{\sin \gamma_{1B}/2} \frac{\sin n_2 \gamma_{2B}/2}{\sin \gamma_{2B}/2} \frac{\sin n_3 \gamma_{3B}/2}{\sin \gamma_{3B}/2} e^{-i[(n_1 - 1)\gamma_{1B}/2 + (n_2 - 1)\gamma_{2B}/2 + (n_3 - 1)\gamma_{3B}/2]} \quad (81)$$

For any point  $P(\theta, \phi)$ , and for beams formed by circuits of the type shown in Figure 11, the arguments of the exponential terms of Eq. (80) and Eq. (81) become

$$\delta_{1A} + \delta_{2A} + \delta_{3A} + \frac{(n_1 - 1)}{2} (k a_1 \sin \theta \cos \phi + \alpha_{1A}) + \frac{(n_2 - 1)}{2} (k a_2 \sin \theta \sin \phi + \alpha_{2A}) + \frac{(n_3 - 1)}{2} (k a_3 \cos \theta + \alpha_{3A}) \quad (82)$$

$$\begin{aligned}
& \delta_{1B} + \delta_{2B} + \delta_{3B} + \frac{(n_1 - 1)}{2} (k a_1 \sin \theta \cos \phi + \alpha_{1B}) + \frac{(n_2 - 1)}{2} (k a_2 \sin \theta \sin \phi + \alpha_{2B}) \\
& + \frac{(n_3 - 1)}{2} (k a_3 \cos \theta + \alpha_{3B})
\end{aligned} \tag{83}$$

A square array implies  $n_2 = n_3 = n$  ; a perfect image plane implies  $\delta_{1A} = \delta_{1B}$ ,  $\alpha_{1A} = \alpha_{1B} = \pi$ ;  $n_1 = 2$ . Since all space terms cancel, the phase difference for the resultant far-fields of beams A and B, referenced to an end source element can be written as

$$\psi = \left[ \delta_{2B} - \delta_{2A} + \delta_{3B} - \delta_{3A} + \frac{(n - 1)}{2} (\alpha_{2B} - \alpha_{2A} + \alpha_{3B} - \alpha_{3A}) \right]. \tag{84}$$

Referring to Figure 11, arbitrarily assume the selection of two adjacent beams so that  $\alpha_{2A} \neq \alpha_{2B}$ , but  $\alpha_{3A} = \alpha_{3B}$ . It is clear from the circuit that this implies that only one horizontal  $_{16,1}S_{ij}$  is energized, but all vertical  $_{16,1}S_{ij}$  are energized (transmitting case) and all radiators are energized. Also, since the adjacent beam signals enter the vertical  $_{16,1}S_{ij}$  at the same level, the delay  $\delta_{3B}$ . The phase difference in this instance reduces to

$$\psi = \delta_{2B} - \delta_{2A} + \frac{(n - 1)}{2} (\alpha_{2B} - \alpha_{2A}). \tag{85}$$

The term  $\psi$ , above, is graphically presented in Figure 13 for  ${}_{16,1}S_{ij}$  when the adjacent beams are generated by columns 248 and 256 of  $C_{ij}$  in  ${}_{16,16}S_{ij}$  given in Eq. (76). The origin and physical significance of the terms  $(\delta_{2B} - \delta_{2A})$  and  $\frac{(n-1)}{2}(\alpha_{2B} - \alpha_{2A})$  are based on the fact that aperture phase is referenced to the source element at the origin of coordinates. Although  $\psi$  was derived from beam considerations in space, it is noted that all space factors are absent in the expression for  $\psi$  and only circuit parameters of  ${}_{16,1}S_{ij}$  remain. It can therefore

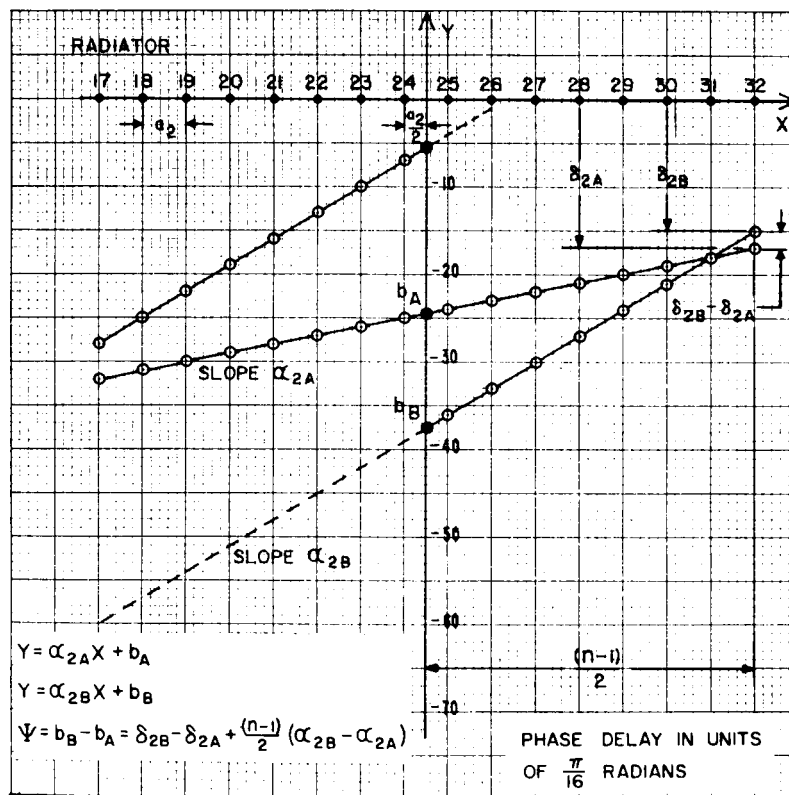


Figure 13—Graphic phase-center determination of  ${}_{16,16}S_{ij}$  beams using  ${}_{16,1}S_{ij}$  scattering matrix gradients.



be taken as the difference between the phase centers  $C_A$  and  $C_B$  of the array beams A and B since  $\psi = C_B - C_A$ . Thus it can be seen that delay is a problem. If these beams are to be used to form a simple sum beam, a phase delay of  $(\psi)$  radians is required in the feeder of beam A. Similarly,  $(\psi + \pi)$  radians of phase delay is required for a simple difference beam.

## APERTURE ILLUMINATION

Originally uniform aperture-element illumination was assumed for each independent transmitting beam formed by a simultaneous beam-forming matrix. This assumption was fundamental to the summation of the polygon of electric field components from the aperture, a geometric series. It is of some interest to investigate the aperture current distribution associated with the formation of sum beams as this provides intermediate beams in space and is prerequisite to more advanced concepts such as phased array monopulse. If the summation involves equal beam weights (i.e., equal principal maxima), equal coefficients can be assigned to the column matrices of  $C_{ij}$  for each beam. Continuing with the planar example, the aperture current is obtained for the particular case of  $\alpha_{3A} = \alpha_{3B} = \pi/16$ ,  $\alpha_{2A} = \pi/16$ ,  $\alpha_{2B} = 3\pi/16$ . For this case

$$\psi = \delta_{2B} - \delta_{2A} + \frac{(n-1)}{2} (\alpha_{2B} - \alpha_{2A}) \quad (85)$$

so that

$$\psi_{248,256} = \frac{15\pi}{16} - \frac{17\pi}{16} + \frac{(16-1)}{2} \left( \frac{3\pi}{16} - \frac{\pi}{16} \right) = 13\pi/16.$$

The current amplitude distribution on the aperture is then obtained by summing the column matrices of  $C_{ij}$  in  $[P_{kk}] [{}_{16,16}S_{ij}] [P_{kk}]$  and  $[{}_{16,16}S_{ij}]$  corresponding to the beams A and B, respectively, where  $P_{kk}$  is a diagonal matrix

with all null elements excepting the principal diagonal. All  $P_{kk} = 1$  except  $P_{256,256} = e^{-j\psi_{248,256}}$  which corresponds to a translation of the reference plane in forming the A beam by excitation of input (256) of  $_{16,16}S_{ij}$ . The B beam is formed by direct excitation of input (248).

Each element of the column matrix  $C_{ij}$  is therefore delayed in phase by an amount  $\psi_{248,256} = 13\pi/16$ . The current amplitude (I) on the aperture when beams A and B coexist, and are properly phased, is given by a sum of column matrices:

$$\begin{bmatrix} C_{257,248} \\ C_{258,248} \\ \vdots \\ C_{511,248} \\ C_{512,248} \end{bmatrix} + \begin{bmatrix} C_{257,256} e^{-j\psi_{248,256}} \\ C_{258,256} e^{-j\psi_{248,256}} \\ \vdots \\ C_{511,256} e^{-j\psi_{248,256}} \\ C_{512,256} e^{-j\psi_{248,256}} \end{bmatrix} = \begin{bmatrix} I_{257} \\ I_{258} \\ \vdots \\ I_{511} \\ I_{512} \end{bmatrix} \quad (86)$$

Figure 14 illustrates the discrete transmitting aperture current amplitude distribution for the sum of beams A and B generated by the previously assumed values of  $\alpha_3$  and  $\alpha_2$ . The current is uniform in the  $\alpha_3$  direction, but has a cosinusoidal envelope in the  $\alpha_2$  direction. This result holds for adjacent beams with equal excitation. The current amplitude can be plotted directly, now, by generating cross-sections of the distribution using the simple rule that the angle between source element current of beams A and B is given by

$$\Phi = x(\alpha_B - \alpha_A) \quad (87)$$

where  $\alpha$  represents the slope of the linear aperture phase plot of Figure 13, and

$x$  is the distance to a radiator from the array center in units of  $a_2$ . Cuts of Figure 14 also represent the current distribution for a linear array of 16 source elements for equal-weight beam addition. The corresponding sum and difference electric field patterns associated with this current distribution are shown in Figure 15.

Certain interesting similarities and differences exist between the transmitting and receiving modes of operation. In forming a single transmitting beam with the  $16 \times 16$  planar array in the previous example, the aperture illumination is uniform and a single input energizes 256 output terminals of  ${}_{16,16}S_{ij}$ . In

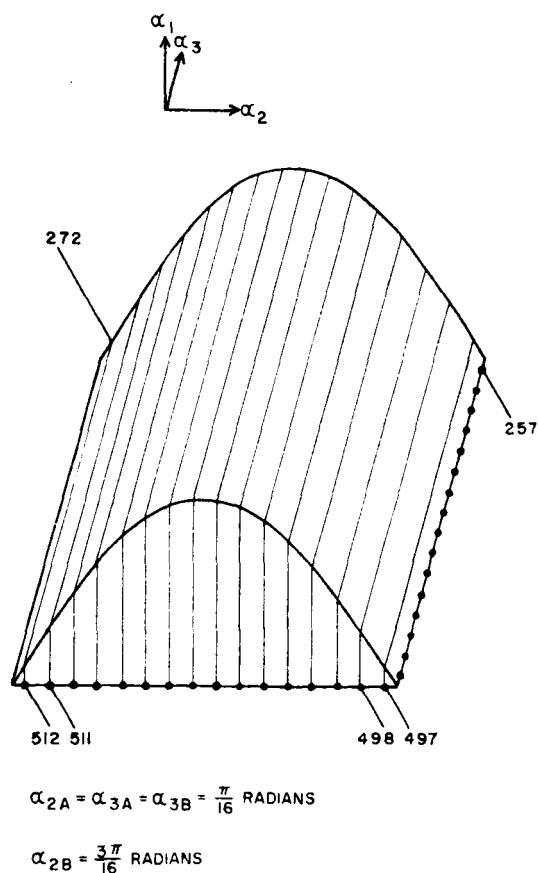


Figure 14—Envelope of planar aperture current distribution resulting from summation of a pair of equally weighted, adjacent, orthogonal transmitting beams.

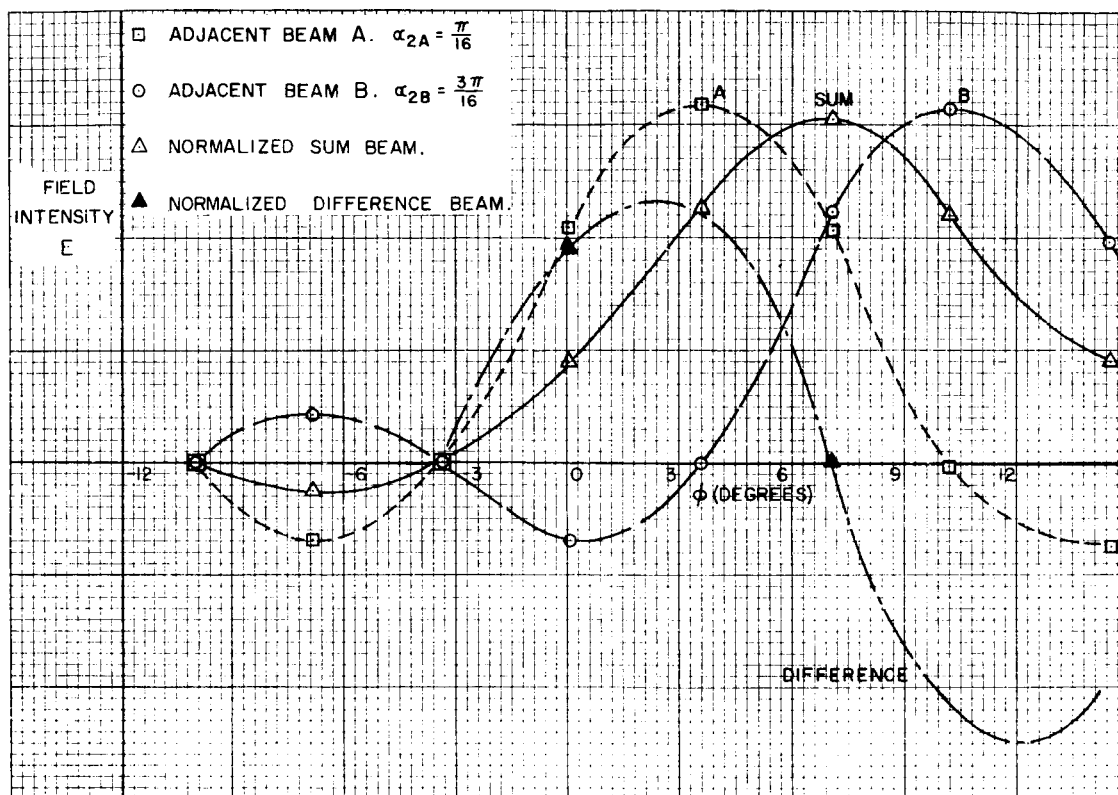


Figure 15—Sum and difference pattern formation of 16 X 1 (linear) array of half-wave dipole elements (H-plane cut).  $a_1 = a_2 = \lambda/2$ .

receiving a single planar wavefront there exist 256 equal signals at the aperture and (256) signals at the beam ports. The transmitting and receiving patterns are identical for these two cases, as are the aperture current distributions. It is noted that the current distribution on the aperture is not necessarily the same for all transmitting/receiving modes for which the patterns are identical. A first-order cosine beam is associated with uniform aperture illumination on reception, but cosine-uniform illumination (as in Figure 14) during transmission if two adjacent beams are summed with equal weight in a planar array.

## CONCLUSION

This report represents an attempt to obtain a realistic description of the far-field radiation patterns for a uniform planar array and, in particular, concerns itself with combinations of gradients obtained from a passive multiple beam-forming matrix. Although the array factors mentioned herein can be found in many textbooks, and elsewhere in the literature, the viewpoint that a uniform planar array is representable as a three-dimensional lattice of oscillators appears to be less common in the antenna literature. For many purposes this is a useful notion. It is possible to analyze the position of beam maxima, nulls, crossover levels, etc. without actually plotting the field patterns. Distinctions are easily made between non-realizable beams (or spurious beams) and grating lobes. The role of the element source pattern can be seen very clearly and the artifice of isotropic element source patterns can be avoided. Finally, the diffraction power-patterns are formed for physically realizable element source factors and three lattice factors, and are then integrated over the hypothetical unit sphere to obtain the total radiated power for various combinations of element spacing and phase gradients. A weighting or normalization of the diffraction patterns is then applied consistent with energy conservation, providing a realistic measure of directive gain.

The introduction of the scattering matrix notation for multiple-beam formation by passive circuits is useful to display the natural order in the signal-processing circuit. Scattering concepts are of proven value in many physical disciplines and particularly in the analysis of electrical circuits. They are not essential to array analysis or to the understanding of multiple beam-forming

matrices. Although the full benefit of the scattering notation may not be evident from the limited discussion given in this report, an examination of the cited references makes clear the extent to which the basic concepts can be carried in the analysis problem. As a specific example scattering matrices can readily be converted into transfer or chain matrices which admit the possibility of tandem-connected circuits. Many other advantages could be cited. These lead to a specialized discussion of eigenvalues, eigenvectors, canonical forms, Pauli spin operators, and related topics in linear algebra and topology. The value of formulating the beam-forming technique is that a very large body of mathematical operations becomes applicable.

This report is planned as the first of a series of reports on the subject of phased arrays and passive scattering matrices, and represents an attempt at unifying some of the topics of elementary planar antenna array system analysis. It is intended to serve as a point of departure into more sophisticated treatments of the overall subject. Less idealized arrays can be investigated within the framework of the notation developed, and more complex systems can subsequently be described by utilizing the basic concepts presented. Subjects such as phased array monopulse, high-order cosine taper illumination, aperture gain, reactive aperture power, array energy conservation, and mutual coupling phenomena constitute logical extensions of the present report. An extensive study of microwave scattering junction topology and basic coupling techniques appears essential to achieving increased design flexibility in phased array systems.

## ACKNOWLEDGMENTS

The author wishes to acknowledge his indebtedness to the following personnel of the Goddard Space Flight Center: A. D. Elia for many valuable discussions, assistance in evaluating mathematical formulae, and a review of the first draft; W. A. Welch for several formal mathematical proofs and the derivation of the crossed-dipole fields; and L. R. Dod for an unusually thorough review and critique of the entire paper.

## References

1. Buerger, M. J., "Crystal-Structure Analysis," New York: John Wiley & Sons, Inc., 1960.
2. Stratton, J. A., "Electromagnetic Theory," New York: McGraw-Hill, 1949.
3. Silver, S., "Microwave Antenna Theory and Design," New York: McGraw-Hill, 1949.
4. Morse, P. M. and Feshbach, "Methods of Theoretical Physics," New York: McGraw-Hill, 1953.
5. Buerger, M. J., "X-ray Crystallography," New York: John Wiley and Sons.
6. Kraus, J. D., "Antennas," New York: McGraw-Hill, 1950.
7. Smullin, L. and Montgomery, C., "Microwave Diplexers," New York: McGraw-Hill, 1948.
8. Montgomery, C., Dicke, B. and Purcell, E., "Principles of Microwave Circuits," New York: McGraw-Hill, 1948.
9. Gantmacher, F.R., "The Theory of Matrices" New York: Chelsea Publishing Company, 1960.
10. Lomont, J. S., "Applications of Finite Groups," New York: Academic Press, 1959.
11. Lax, B. and Button, K. J., "Microwave Ferrites and Ferrimagnetics," New York: McGraw-Hill, 1962.

12. Hadley, G., "Linear Algebra" Reading, Mass.: Addison-Wesley Publishing Company, 1961.
13. Skolnik, M. L., "Introduction to Radar Systems," New York: McGraw-Hill, 1962.
14. Stone, J. M., "Radiation and Optics," New York: McGraw-Hill, 1963.
15. "Multidirectional Beam Scanning Antenna Array Report" (Final Report) by W. L. Maxon Corporation (1959-1960), AD 254051.
16. "Phased Array Radar Studies" by Massachusetts Institute of Technology Lincoln Laboratory (1960-1961), AD 271724.
17. "Applications of Group Theory in the Study of Symmetrical Waveguide Junctions," by B. A. Auld (1952), Stanford University, TIP 22478.
18. "Linear Arrays with Arbitrarily Distributed Elements" by H. Unz (1956), AD 118981.
19. "Multi-dimensional Lattice Arrays with Arbitrarily Distributed Elements," by H. Unz (1956), AD 121880.
20. "Scanning Techniques for Large Flat Communication Antenna Arrays," by Shelton, Perrino, and Davis (1960), AD 235571.
21. "Cross-Coupling in Multiple Beam Antennas," by Sylvania Electronic Systems (1961), AD 257485.
22. "An RF Multiple Beam Forming Technique" by W. P. Delaney, Massachusetts Institute of Technology Lincoln Laboratory (1961), AD 262017.
23. "The Theory and Application of the Scattering Matrix for Electromagnetic Waves" by R. Tsu, Ohio State University, (1960), AD 243 689.
24. "Phased Array Radar Studies" by Massachusetts Institute of Technology Lincoln Laboratory (1959-1960), AD 249 470.
25. Polytechnic Institute of Brooklyn, Microwave Research Institute Symposia Series; "I Modern Network Synthesis," "IV Modern Advances in Microwave Techniques", New York: Polytechnic Press, 1952, 1954.



## Appendix A

### Radiation Pattern of Crossed-Dipole Antennas

The radiated fields of the crossed dipole antenna shown in Figure (1) can be determined by the Poynting integration method.<sup>1</sup> The radiation vector from a linear antenna is given by

$$\vec{N} = \int \vec{i}_\ell e^{jk|\vec{r}'|\cos\psi} d\ell \quad (1)$$

where  $|\vec{r}'|$  = radius from origin to differential element,  $d\ell$ , on the antenna

$|\vec{r}|$  = radius from origin to the point P at which the field is to be calculated

$\psi$  = angle between  $\vec{r}$  and  $\vec{r}'$

and the time dependent factor  $e^{j\omega t}$  is understood (i.e., omitted). The vector potential at point P is

$$\vec{A} = \mu \frac{e^{-jk r}}{4\pi r} \vec{N} \quad (2)$$

and the fields at point P are given by

$$\vec{E} = -\frac{j\omega}{k^2} \nabla(\nabla \cdot \vec{A}) - j\omega \vec{A} \quad (3)$$

$$\vec{B} = \nabla \times \vec{A}$$

---

<sup>1</sup>Ramo, S. and Whinnery, J., "Fields and Waves in Modern Radio", New York: John Wiley and Sons, Inc., 1953. p. 505 ff.

The only components of the above fields which do not decrease faster than  $1/r$  are

$$\begin{aligned} E_{\theta} &= \frac{-j\omega\mu}{4\pi r} e^{-jk r} N_{\theta} & E_{\phi} &= \frac{-j\omega\mu}{4\pi r} e^{-jk r} N_{\phi} \\ H_{\theta} &= \frac{jk}{4\pi r} e^{-jk r} N_{\phi} & H_{\phi} &= \frac{-jk}{4\pi r} e^{-jk r} N_{\theta} \end{aligned} \quad (4)$$

For a specified antenna configuration and current distribution, equations (1) and (4) can be solved for the components of the radiated fields. For the crossed-dipole antenna with half-wave dipole elements and an assumed sinusoidal current distribution, the radiation functions (components of the radiation vector) are shown in Appendix A to be

$$\begin{aligned} N_{\theta}(\theta_a, \theta, \phi) &= \frac{2I_0}{k} \left[ \frac{\cos\left(\frac{\pi}{2}\alpha\right)}{1-\alpha^2} (\sin\phi \cos\theta \sin\theta_a - \sin\theta \cos\theta_a) \right] \\ &+ \frac{2I_0}{k} \left[ \frac{\cos\left(\frac{\pi}{2}\beta\right)}{1-\beta^2} e^{-j\gamma} (\sin\phi \cos\theta \cos\theta_a + \sin\theta \sin\theta_a) \right] \end{aligned} \quad (5)$$

$$N_{\phi}(\theta_a, \theta, \phi) = \frac{2I_0}{k} \cos\phi \left[ \frac{\sin\theta_a \cos\left(\frac{\pi}{2}\alpha\right)}{1-\alpha^2} + \frac{\cos\theta_a \cos\left(\frac{\pi}{2}\beta\right)}{1-\beta^2} e^{-j\gamma} \right] \quad (6)$$

where  $\gamma$  = difference in phase of the currents on the individual dipoles

$$\alpha = \cos\theta \cos\theta_a + \sin\theta \sin\theta_a \sin\phi$$

$$\beta = \cos\theta \sin\theta_a - \sin\theta \cos\theta_a \sin\phi$$

$\theta_a$  = tilt angle defined in Figure 1

Substituting for the tilt angle and phase difference in Equations (5) and (6) yields the components of the radiation vector for the desired antenna orientations and polarizations:

1)  $\theta_a = 0^\circ$ ; linear polarization ( $\gamma = 0^\circ$ )

$$N_\theta(0, \theta, \phi) = -\frac{2I_0}{k} \left[ \frac{\cos\left(\frac{\pi}{2} \cos \theta\right)}{\sin \theta} + \frac{\sin \phi \cos \theta \cos\left(\frac{\pi}{2} \sin \theta \sin \phi\right)}{1 - \sin^2 \theta \sin^2 \phi} \right] \quad (7)$$

$$N_\phi(0, \theta, \phi) = -\frac{2I_0}{k} \frac{\cos \phi \cos\left(\frac{\pi}{2} \sin \theta \sin \phi\right)}{1 - \sin^2 \theta \sin^2 \phi} \quad (8)$$

The substitution of  $\phi = 0^\circ$  in Equations (7) and (8) leads to the radiation functions in the E-plane ( $\phi = 0^\circ$  plane) as

$$N_\theta(0, \theta, 0) = -\frac{2I_0}{k} \frac{\cos\left(\frac{\pi}{2} \cos \theta\right)}{\sin \theta} \quad (9)$$

$$N_\phi(0, \theta, 0) = -\frac{2I_0}{k} \quad (10)$$

The substitution of  $\theta = 90^\circ$  in (7) and (8) leads to the radiation functions in the H-plane ( $\theta = 90^\circ$  plane) as

$$N_\theta(0, 90^\circ, \phi) = -\frac{2I_0}{k} \quad (11)$$

$$N_\phi(0, 90^\circ, \phi) = -\frac{2I_0}{k} \frac{\cos\left(\frac{\pi}{2} \sin \phi\right)}{\cos \phi} \quad (12)$$

2)  $\theta_a = 0^\circ$ ; circular polarization ( $\gamma = 90^\circ$ )

$$N_\theta(0, \theta, \phi) = -\frac{2I_0}{k} \left[ \frac{\cos\left(\frac{\pi}{2} \cos \theta\right)}{\sin \theta} + j \frac{\sin \phi \cos \theta \cos\left(\frac{\pi}{2} \sin \theta \sin \phi\right)}{1 - \sin^2 \theta \sin^2 \phi} \right] \quad (13)$$

$$N_\phi(0, \theta, \phi) = j \frac{2I_0}{k} \cos \phi \frac{\cos\left(\frac{\pi}{2} \sin \theta \sin \phi\right)}{1 - \sin^2 \theta \sin^2 \phi} \quad (14)$$

The radiation functions in the E-plane are

$$N_\theta(0, \theta, 0) = -\frac{2I_0}{k} \frac{\cos\left(\frac{\pi}{2} \cos \theta\right)}{\sin \theta} \quad (15)$$

$$N_\phi(0, \theta, 0) = j \frac{2I_0}{k} \quad (16)$$

The radiation functions in the H-plane are

$$N_\theta(0, 90^\circ, \phi) = -\frac{2I_0}{k} \quad (17)$$

$$N_\phi(0, 90^\circ, \phi) = j \frac{2I_0}{k} \frac{\cos\left(\frac{\pi}{2} \sin \phi\right)}{\cos \phi} \quad (18)$$

3)  $\theta_a = 45^\circ$ ; linear polarization ( $\gamma = 0$ )

$$N_\theta(45^\circ, \theta, \phi) = \frac{\sqrt{2}}{k} I_0 \left\{ \frac{\cos \left[ \frac{\pi}{2\sqrt{2}} (\cos \theta + \sin \theta \sin \phi) \right] (\sin \phi \cos \theta - \sin \theta)}{1 - \frac{1}{2} (\cos \theta + \sin \theta \sin \phi)^2} - \frac{\cos \left[ \frac{\pi}{2\sqrt{2}} (\cos \theta - \sin \theta \sin \phi) \right] (\sin \phi \cos \theta + \sin \theta)}{1 - \frac{1}{2} (\cos \theta - \sin \theta \sin \phi)^2} \right\} \quad (19)$$

$$N_\phi(45^\circ, \theta, \phi) = \frac{\sqrt{2}}{k} I_0 \cos \phi \left\{ \frac{\cos \left[ \frac{\pi}{2\sqrt{2}} (\cos \theta + \sin \theta \sin \phi) \right]}{1 - \frac{1}{2} (\cos \theta + \sin \theta \sin \phi)^2} - \frac{\cos \left[ \frac{\pi}{2\sqrt{2}} (\cos \theta - \sin \theta \sin \phi) \right]}{1 - \frac{1}{2} (\cos \theta - \sin \theta \sin \phi)^2} \right\} \quad (20)$$

The radiation functions in the E-plane are

$$N_\theta(45^\circ, \theta, 0) = - \frac{2\sqrt{2}}{k} I_0 \frac{\sin \theta \cos \left( \frac{\pi}{2\sqrt{2}} \cos \theta \right)}{1 - \frac{1}{2} \cos^2 \theta} \quad (21)$$

$$N_\phi(45^\circ, \theta, 0) = 0 \quad (22)$$

and the radiation pattern is plotted in Figure 4.

The radiation functions in the H-plane are

$$N_{\theta}(45^{\circ}, 90^{\circ}, \phi) = -\frac{2\sqrt{2}}{k} I_0 \frac{\cos\left(\frac{\pi}{2\sqrt{2}} \sin \phi\right)}{1 - \frac{1}{2} \sin^2 \phi} \quad (23)$$

$$N_{\phi}(45^{\circ}, 90^{\circ}, \phi) = 0 \quad (24)$$

and the radiation pattern is plotted in Figure 5.

4)  $\theta_a = 45^{\circ}$ ; circular polarization ( $\gamma = \pi/2$ )

$$N_{\theta}(45^{\circ}, \theta, \phi) = \frac{\sqrt{2}}{k} I_0 \left\{ \frac{(\sin \phi \cos \theta - \sin \theta) \cos \left[ \frac{\pi}{2\sqrt{2}} (\cos \theta + \sin \theta \sin \phi) \right]}{1 - \frac{1}{2} (\cos \theta + \sin \theta \sin \phi)^2} \right. \\ \left. + j \frac{(\sin \phi \cos \theta + \sin \theta) \cos \left[ \frac{\pi}{2\sqrt{2}} (\cos \theta - \sin \theta \sin \phi) \right]}{1 - \frac{1}{2} (\cos \theta - \sin \theta \sin \phi)^2} \right\} \quad (25)$$

$$N_{\phi}(45^{\circ}, \theta, \phi) = \frac{\sqrt{2}}{k} I_0 \cos \phi \left\{ \frac{\cos \left[ \frac{\pi}{2\sqrt{2}} (\cos \theta + \sin \theta \sin \phi) \right]}{1 - \frac{1}{2} (\cos \theta + \sin \theta \sin \phi)^2} \right. \\ \left. + j \frac{\cos \left[ \frac{\pi}{2\sqrt{2}} (\cos \theta - \sin \theta \sin \phi) \right]}{1 - \frac{1}{2} (\cos \theta - \sin \theta \sin \phi)^2} \right\} \quad (26)$$

The radiation functions in the E-plane are

$$N_{\theta}(45^{\circ}, \theta, 0) = -\frac{\sqrt{2} I_0}{k} (1 - j) \frac{\sin \theta \cos \left( \frac{\pi}{2\sqrt{2}} \cos \theta \right)}{1 - \frac{1}{2} \cos^2 \theta} \quad (27)$$

$$N_{\phi}(45^{\circ}, \theta, 0) = \frac{\sqrt{2} I_0}{k} (1 + j) \frac{\cos \left( \frac{\pi}{2\sqrt{2}} \cos \theta \right)}{1 - \frac{1}{2} \cos^2 \theta} \quad (28)$$

and the radiation patterns are plotted in Figure 6.

The radiation functions in the H-plane are

$$N_{\theta}(45^{\circ}, 90^{\circ}, \phi) = \frac{\sqrt{2} I_0}{k} \cos \phi (1 + j) \frac{\cos \left[ \frac{\pi}{2\sqrt{2}} \sin \phi \right]}{1 - \frac{1}{2} \sin^2 \phi} \quad (29)$$

$$N_{\phi}(45^{\circ}, 90^{\circ}, \phi) = -\frac{\sqrt{2} I_0}{k} (1 - j) \frac{\cos \left[ \frac{\pi}{2\sqrt{2}} \sin \phi \right]}{1 - \frac{1}{2} \sin^2 \phi} \quad (30)$$

and the radiation patterns are plotted in Figure 7.

Addendum to Appendix A  
Derivation of Radiation Vector for Crossed-Dipole Antennas

For the  $\lambda/2$  dipole oriented along the  $Z'$ -axis (Figure 2) the radiation vector is given by

$$\vec{N}_1 = \int \vec{i}_\ell e^{jk|\vec{r}'| \cos \psi} d\ell = \int_{-\lambda/4}^{\lambda/4} \vec{i}_{z'} e^{jk|z'| \cos \psi} dz'$$

If  $\vec{u}$  and  $\vec{a}_{z'}$  are unit vectors along  $\vec{r}$  and  $\vec{r}'$ , respectively:

$$\vec{u} = \vec{a}_x \sin \theta \cos \phi + \vec{a}_y \sin \theta \sin \phi + \vec{a}_z \cos \theta$$

$$\vec{a}_{z'} = \vec{a}_y \sin \theta_a + \vec{a}_z \cos \theta_a$$

$$\cos \psi = \vec{u} \cdot \vec{v} = \cos \theta \cos \theta_a + \sin \theta \sin \theta_a \sin \phi = \alpha.$$

For a sinusoidal distribution of current

$$\vec{i}_{z'} = \vec{a}_{z'} I_0 \sin \left[ k \left( \frac{\lambda}{4} - |z'| \right) \right] \quad -\frac{\lambda}{4} \leq z' \leq \frac{\lambda}{4}$$

$$\therefore \vec{N}_1 = \vec{a}_{z'} \int_{-\lambda/4}^0 I_0 \sin [k(\ell + z')] e^{jk\alpha z'} dz' + \vec{a}_{z'} \int_0^{\lambda/4} I_0 \sin [k(\ell - z')] e^{jk\alpha z'} dz'$$

$$= \vec{a}_{z'} \frac{2I_0}{k} \frac{\cos \left( \frac{\pi}{2} \alpha \right)}{1 - \alpha^2}$$

$$= \frac{2I_0}{k} \frac{\cos \left( \frac{\pi}{2} \alpha \right)}{1 - \alpha^2} [\vec{a}_y \sin \theta_a + \vec{a}_z \cos \theta_a]$$



If the current for the  $\lambda/2$  dipole along the  $Z''$ -axis (Figure 3) is assumed to be

$$\vec{I}_{z''} = \vec{a}_{z''} I_0 e^{-j\gamma} \sin \left[ k \left( \frac{\lambda}{4} - |z''| \right) \right] \quad -\frac{\lambda}{4} \leq z'' \leq \frac{\lambda}{4}$$

then its radiation vector is determined in like manner to be

$$\vec{N}_2 = \frac{2I_0 e^{-j\gamma}}{k(1-\beta^2)} \cos \left( \frac{\pi}{2} \beta \right) [-\vec{a}_y \cos \theta_a + \vec{a}_z \sin \theta_a]$$

The total radiation vector is

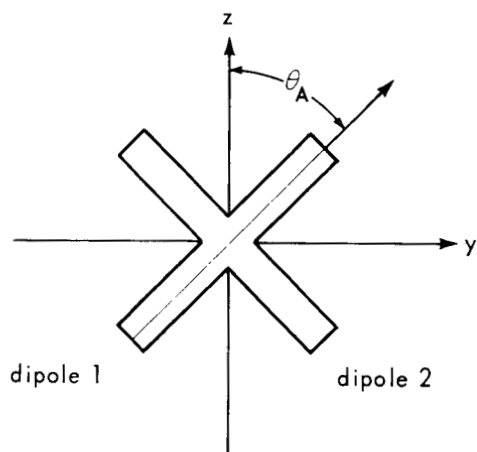
$$\begin{aligned} \vec{N} = \vec{N}_1 + \vec{N}_2 = \vec{a}_y \frac{2I_0}{k} & \left[ \frac{\sin \theta_a \cos \left( \frac{\pi}{2} \alpha \right)}{1-\alpha^2} - \frac{\cos \theta_a \cos \left( \frac{\pi}{2} \beta \right)}{1-\beta^2} \right] \\ & + \vec{a}_z \frac{2I_0}{k} \left[ \frac{\cos \theta_a \cos \left( \frac{\pi}{2} \alpha \right)}{1-\alpha^2} + \frac{\sin \theta_a \cos \left( \frac{\pi}{2} \beta \right)}{1-\beta^2} \right] \end{aligned}$$

and the spherical components are:

$$\begin{aligned} N_\theta &= N_y \sin \phi \cos \theta - N_z \sin \theta \\ &= \frac{2I_0}{k} \left[ \frac{\cos \left( \frac{\pi}{2} \alpha \right)}{1-\alpha^2} (\sin \phi \cos \theta \sin \theta_a - \sin \theta \cos \theta_a) \right] \\ &+ \frac{2I_0}{k} \frac{\cos \left( \frac{\pi}{2} \beta \right)}{1-\beta^2} e^{-j\gamma} (\sin \phi \cos \theta \cos \theta_a + \sin \theta \sin \theta_a) \end{aligned}$$

$$N_\phi = N_y \cos \phi$$

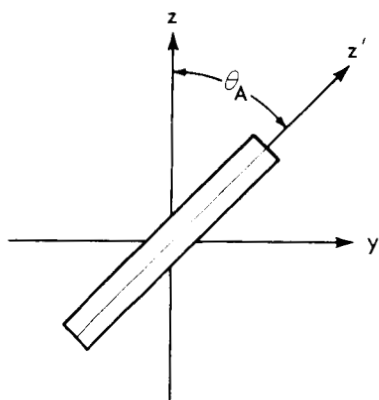
$$= \frac{2I_0}{k} \cos \phi \left[ \frac{\sin \theta_a \cos \left( \frac{\pi}{2} \alpha \right)}{1-\alpha^2} + \frac{\cos \theta_a \cos \left( \frac{\pi}{2} \beta \right) e^{-j\gamma}}{1-\beta^2} \right]$$



$$0 \leq \theta_A \leq \frac{\pi}{2}$$

1. Length of each dipole  $\frac{\lambda}{2}$

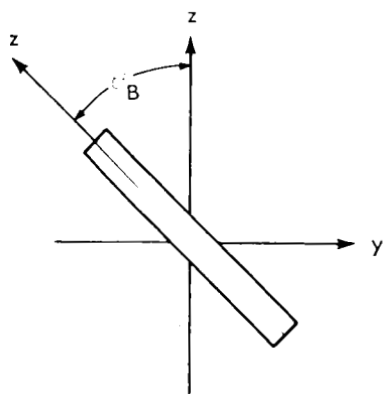
Figure 1-Crossed-Dipole Antenna.



$$\vec{r}' = a_z' z'$$

$$= a_y z' \sin A + a_z z' \cos A$$

Figure 2-Geometry for Calculation of Radiation Vector Due to Dipole 1.



$$B = \frac{\pi}{2} - A$$

$$\vec{r}'' = a_z'' z''$$

$$= a_y z'' \sin B + a_z z'' \cos B$$

$$= a_y z'' \cos A + a_z z'' \sin A$$

Figure 3-Geometry for Calculation of Radiation Vector Due to Dipole 2.

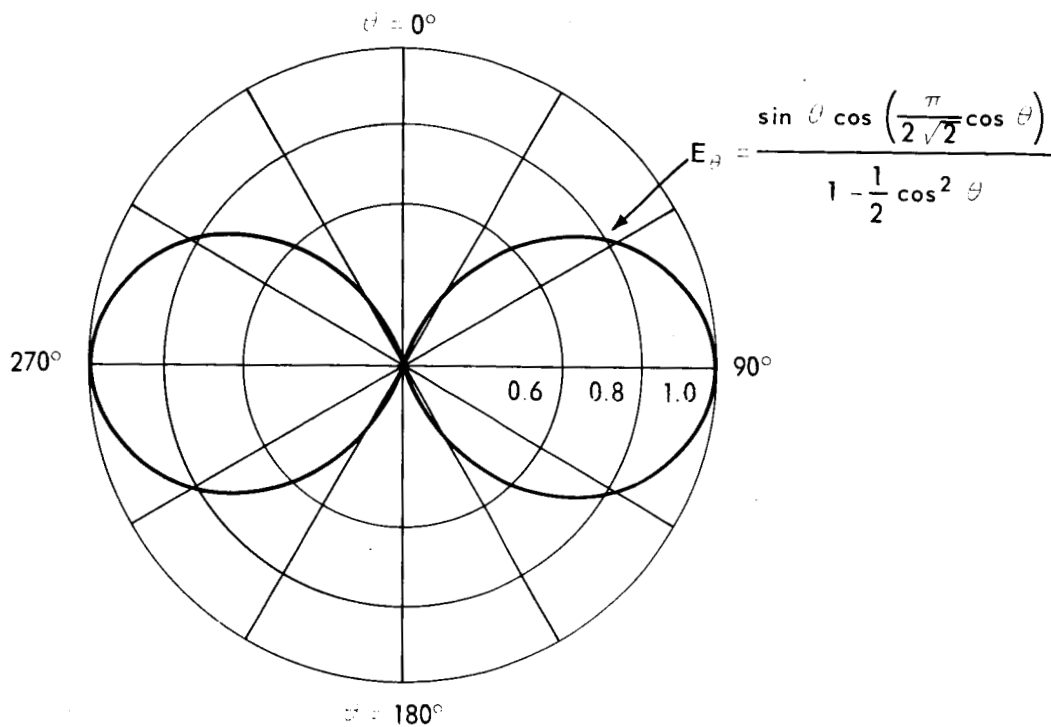


Figure 4—Radiation Pattern on E-Plane for  $\theta_A = 45^\circ$ ,  $\gamma = 0^\circ$ .

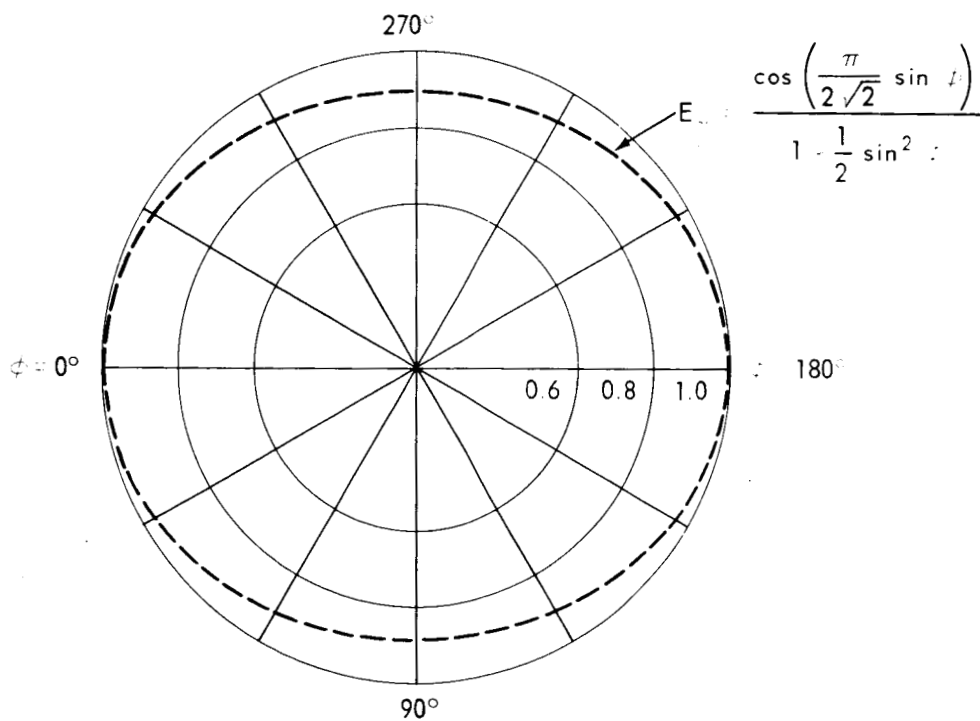


Figure 5—Radiation Pattern on H-Plane for  $\theta_A = 45^\circ$ ,  $\gamma = 0^\circ$ .

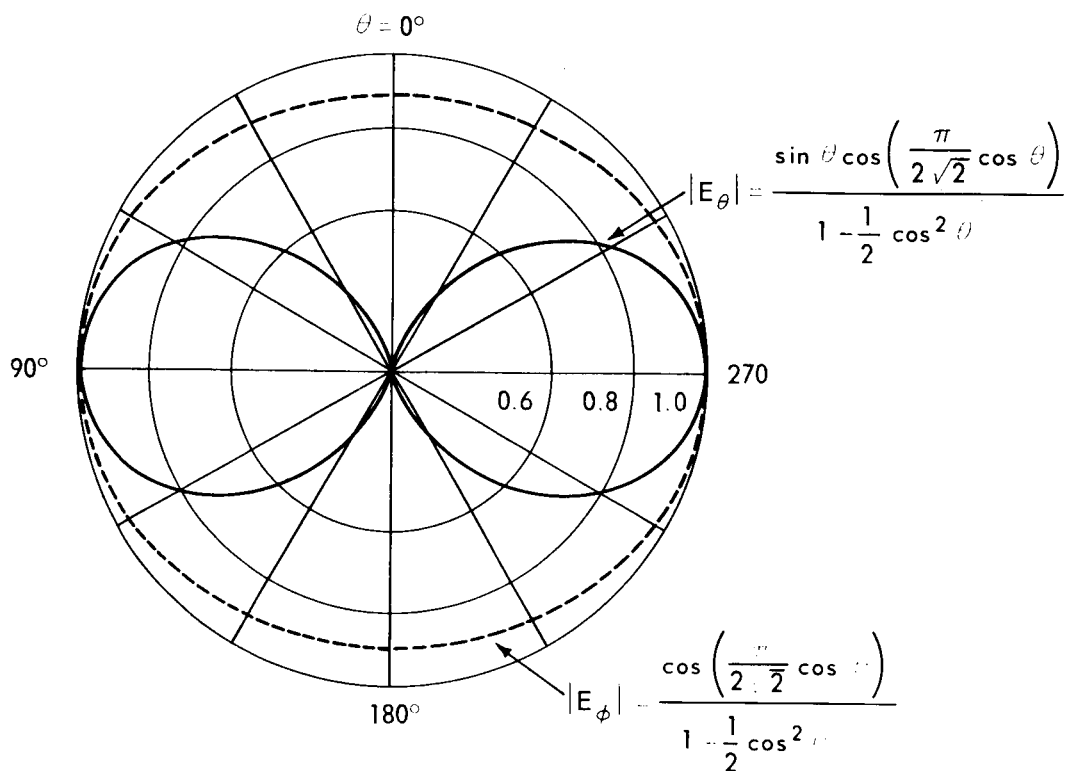


Figure 6-Radiation Patterns on E-Plane for  $\theta_A = 45^\circ$ ,  $\gamma = 90^\circ$ .

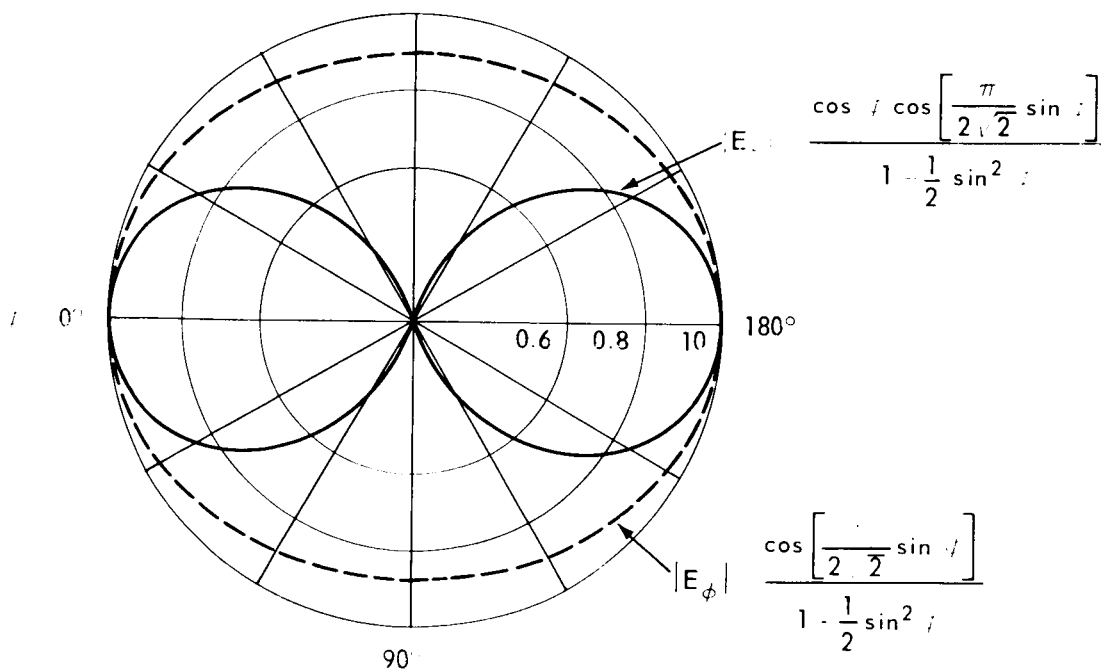


Figure 7-Radiation Patterns on H-Plane for  $\theta_A = 45^\circ$ ,  $\gamma = 90^\circ$ .